Reviews of Geophysics

REVIEW ARTICLE
10.1029/2020RG000732

Key Points:

- Extreme regional rainfall anomalies, were a recurrent feature of marine isotope stages 2–4
- Anomalies resulted from the southward displacement of the Hadley circulation and the Intertropical Convergence Zone
- Anomalies occurred when ice-rafted debris was deposited in the N. Atlantic, as freshwater reduced the North Atlantic Overturning Circulation

Correspondence to:
R. S. Bradley,
rbradley@geo.umass.edu

Citation:
Bradley, R. S., & Diaz, H. F. (2021). Late Quaternary abrupt climate change in the tropics and sub-tropics: The continental signal of Tropical Hydroclimatic Events (THEs). *Reviews of Geophysics*, *59*, e2020RG000732. https://doi.org/10.1029/2020RG000732

Received 23 FEB 2021
Accepted 11 SEP 2021

Late Quaternary Abrupt Climate Change in the Tropics and Sub-Tropics: The Continental Signal of Tropical Hydroclimatic Events (THEs)

Raymond S. Bradley[1] **and Henry F. Diaz**[2]

[1]Department of Geosciences, University of Massachusetts, Amherst, MA, USA, [2]Department of Geography and Environment, University of Hawaii, Manoa, HI, USA

Abstract

Tropical hydroclimatic events, characterized by extreme regional rainfall anomalies, were a recurrent feature of marine isotope stages 2–4 and involved some of the most abrupt and dramatic climatic changes in the late Quaternary. These anomalies were pervasive throughout the tropics and resulted from the southward displacement of the Hadley circulation and the Intertropical Convergence Zone (ITCZ) and its associated convective rainfall, modulated by regional factors. Lake sediments, stalagmites, and offshore marine sediments that integrate inland continental conditions provide a comprehensive record of these changes over the past ~70,000 yr. Vast areas experienced severe drought while other areas recorded greatly increased rainfall. Within the uncertainties of dating, these tropical rainfall anomalies occurred very close in time ($\pm 10^2$–10^3 yr) to the deposition of North Atlantic ice-rafted debris (IRD) that defines Heinrich events (HEs). The IRD record is a good proxy for the amount and distribution of additional freshwater forcing which was necessary to bring about a drastic reduction in the Atlantic Meridional Overturning Circulation (AMOC) strength during each HE. As a consequence of this reduction in AMOC and an abrupt expansion in the area of sea-ice, cooling of the North Atlantic and adjacent continents took place, with a rapid atmospheric response involving the southward displacement of the ITCZ and associated rainfall belts. The climatic consequences of this large-scale change in the Hadley circulation, modulated by regional factors, is clearly recorded throughout the tropics as a series of abrupt and extreme hydroclimatic events. Some of the physical mechanisms that may have played a role in those changes are discussed.

Plain Language Summary

Many continental paleoclimate records from the inter-tropical zone show that there were occasional abrupt changes in rainfall across the region that we call "Tropical Hydroclimatic Events." These extraordinary climate changes occurred throughout the tropics, with excessive rainfall in some areas, while at the same time other regions experienced severe drought. These events resulted from large outflows of freshwater into the North Atlantic. The sudden freshening of the subpolar North Atlantic led to a slow-down or cessation in deepwater formation: the Atlantic Meridional Overturning Circulation (AMOC). This led to a rapid reduction in the northward flux of heat by the ocean in the poleward flowing Gulf Stream current, which in turn led to a reorganization of the atmospheric general circulation, modifying the climate in various parts of the world. The consequences of the large and sudden flux of freshwater to the North Atlantic leading to a collapse of the AMOC caused major rain belts across the tropics to shift southward, but this large-scale atmospheric response had different regional consequences. We provide an overview of these sudden changes in tropical climates around the world and considers some of the physical mechanisms that may have played a role in those changes.

1. Introduction

The focus of this review is on the climate of tropical and sub-tropical regions at times when ice-rafted sediments (IRD) were carried into the North Atlantic and deposited over large areas, mainly between 40°N and 55°N (in the "Ruddiman Belt"; Kissel, 2005). Around these times, large and abrupt changes in hydroclimate (resulting from major changes in rainfall amount) were widespread across all low latitude regions. These changes are distinct from other abrupt changes that are associated with Dansgaard-Oeschger (DO) events seen in ice cores (Corrick et al., 2020).

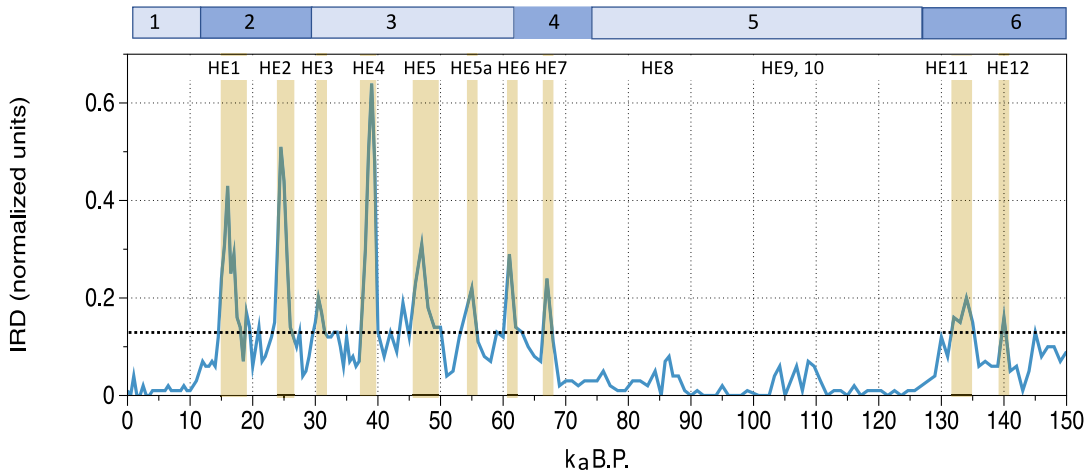

Figure 1. North Atlantic IRD stack derived from 15 individual sediment cores (arbitrary units scaled to a maximum of 1). Brown-shaded range indicates time periods when IRD values exceeded the median value (0.13: black dashed line) for 13–70 ka B.P. (data from Lisiecki & Stern, 2016). Marine isotope stages indicated at the top. Note that the timing and magnitude of IRD maxima vary from one location to another, and only 5 cores extend back before MIS4. For 0–40 ka B.P., the dating is based on radiocarbon (interpolated to 500 yr intervals); dating of the 40–150 ka portion of the stack is by correlation to GICC05 and speleothem age models and interpolated to 1000 yr intervals. Data source: https://doi.org/10.1002/2016PA003002; Supp data set S1: palo20372-sup-003-ds01.txt.

To clarify the terminology used here: the IRD is recognized by distinct facies changes in North Atlantic sediment cores—stratigraphically, these are **Heinrich layers**. Since these layers appear to have been deposited within a relatively short period of time, the term **Heinrich event** (HE) describes these depositional time intervals. However, not all HEs were the same; some appear to have been abrupt and singular events (such as HE4) whereas others had multiple phases (cf. Hodell et al., 2017). This is as illustrated in Figure 1, which shows a stack of IRD records from the North Atlantic (Lisiecki & Stern, 2016). We will use this record throughout the article to compare with paleoclimatic evidence from low latitudes, but several limitations should be noted. First, the timing and magnitude of IRD maxima varied from one location to another across the Ruddiman Belt (see Figure S2 in Lisiecki & Stern, 2016, and the Discussion section below) and stacking such data may obscure the detailed sequence of deposition within an event. Second, for 0–40 ka B.P., the dating is based on radiocarbon (interpolated to 500 yr intervals) whereas dating of the 40–150 ka portion of the stack is by correlation to GICC05 (the Greenland ice core 2005 chronology) and speleothem age models, and interpolated to 1000 yr intervals. Third, only five of the selected cores extend back before MIS4. While the timing of maximum IRD deposition in this composite record is fairly clear, defining precisely when HEs began, and when they ended is more problematical and compounded by the uncertainties involved in radiocarbon dating marine sediments, leading to a range of published estimates (Table 1). In the figures of this article, the time of IRD maximum and the interval when IRD exceeded the median in MIS2–4 will be indicated, based on the Lisiecki and Stern stack.

Since Heinrich layers are presumably associated with freshwater forcing (from melting icebergs that delivered the IRD to the North Atlantic) and such forcing is linked to a reduction in Atlantic Meridional Overturning Circulation (AMOC) strength (see Discussion), some have used the term **Heinrich stadial** to describe a period of reduced AMOC and associated cooling. In fact, North Atlantic cooling often preceded the deposition of IRD so the use of this term is confusing, and especially so when "Heinrich" is applied to an overall period of cooling (a stadial), which may have begun long before the deposition of IRD (Heinrich layers). Furthermore, as a reduction in AMOC leads to warming in the southern hemisphere, it seems illogical to link the word "Heinrich" to a stadial at all, and so (as suggested by Andrews & Voelker, 2018), it probably should be abandoned. By the same token, it is inappropriate to label a rainfall anomaly in the tropics a "HE" (even if roughly synchronous with HEs), since HEs are defined by the deposition of IRD in the extra-tropical North Atlantic.

Table 1
Timing of Heinrich Layers (ka B.P.)

Sources:	1	1b	2	3	4	5	6*
HE1	16.0	18–15	16.4–16.2	17.25–16	18.0–15.6	15.6–15.2 (HI.2)	16.13–14.615
						16.5–16.2 (**H1.1**)	
HE2	24.5	26–23.5	24.2–24	25.2–24	26.5–24.3		24.03–23.292
HE3..	30.5	31–30	32.2	~31	32.7–31.3		
HE4	39.0	37.5–39.5	39.2–38.1	~38	40.2–38.3		39.54–38.42
HE5	47.0	50–46	48.4–45.8	~45	50–47		48.39–47.101
HE5a	55.0	55–54					
HE6	61.0	62–61	60.6	~60	63.2–60.1		
HE7	67.0	67	67.8				
HE8	~86						
HE9	~107						
HE10	~109						
HE11	~134.	135–132					
HE12	~140	140					

Note. 1. Lisiecki and Stern (2016): Peak IRD in stack of 15 records (interpolated to 500 yr intervals up to 40 ka B.P. and 1,000 yr intervals before that). 1b. Range of stacked IRD values >0.13 (median value for 13–70 ka B.P.). 2. Zhou et al. (2021): $^{230}Th_{xs}$ minima in JPC37 (43°58'N, 46°25'W, 3,981 m). 3. Hemming (2004): based on %IRD in a number of N. Atlantic sediment cores; dating of HE1 and 2 based on ^{14}C; others correlated to Greenland ice core $\delta^{18}O$. 4. Sanchez-Goñi and Harrison (2010): "Heinrich stadials". 5. Hodell et al. (2017). 6. Rhodes et al. (2015) (*Antarctic ice core methane, indicating tropical wetland expansion in the southern hemisphere).

In this article, abrupt and significant rainfall changes in the tropics and sub-tropics are referred to as **Tropical Hydroclimatic Events (THEs)**. We consider continental records that provide evidence for one or more THEs in MIS 2–4. There are many more records of the most recent THE (corresponding to HE1) than for earlier events, and less agreement about the timing of earlier THEs. Although there may have been THEs (and related HEs) during MIS5 or during earlier marine isotope stages (cf. Channell et al., 2012; Hodell, Channell, et al., 2008; Martrat et al., 2007; McManus et al., 1999), here the focus is on the most recent 5 or 6 events which occurred during the last ~70 ka (Figure 1). Generally, the archives considered are either lake sediments (if well-dated) or stalagmites, though occasionally marine sediments that have recorded some aspect of conditions on the adjacent continents are also considered (Figure 2). As with marine sediments, there are often difficulties in precisely dating abrupt changes seen in lake sediments, but THEs can generally be dated very precisely in stalagmites by the use of U-series dating methods (with uncertainties on the order of only a few decades, in some cases). Geographically, the domain being considered is the area between the Tropics of Cancer and Capricorn though other records relevant to conditions in that region are included when appropriate.

2. Controls on Tropical and Sub-Tropical Climate

The climate of the tropics and sub-tropics is dominated by the Hadley circulation, which creates distinct *seasonal* changes, and strong *regional* variations in rainfall related to passage of the sun overhead (Figure 3). During the equinoctial seasons, the Hadley circulation has two distinct cells, with the ascending limb (the Intertropical Convergence Zone, ITCZ), positioned slightly north of the Equator today, on average, and areas of subsidence to the north and south in the sub-tropics. However, in the solstitial seasons, there is only one cell, with the area of low-level convergence and rising air shifting from north of the Equator in boreal summer to south of the Equator in boreal winter, and a corresponding hemispheric shift in the zone of subsidence (Webster, 2005; Figure 3). Net heat transport is oriented in the direction of motion in the upper branch of the Hadley cell where moist static energy exceeds that at the surface. Thus, energy is transported away from the ITCZ, so when the ITCZ is displaced toward the southern hemisphere (in austral

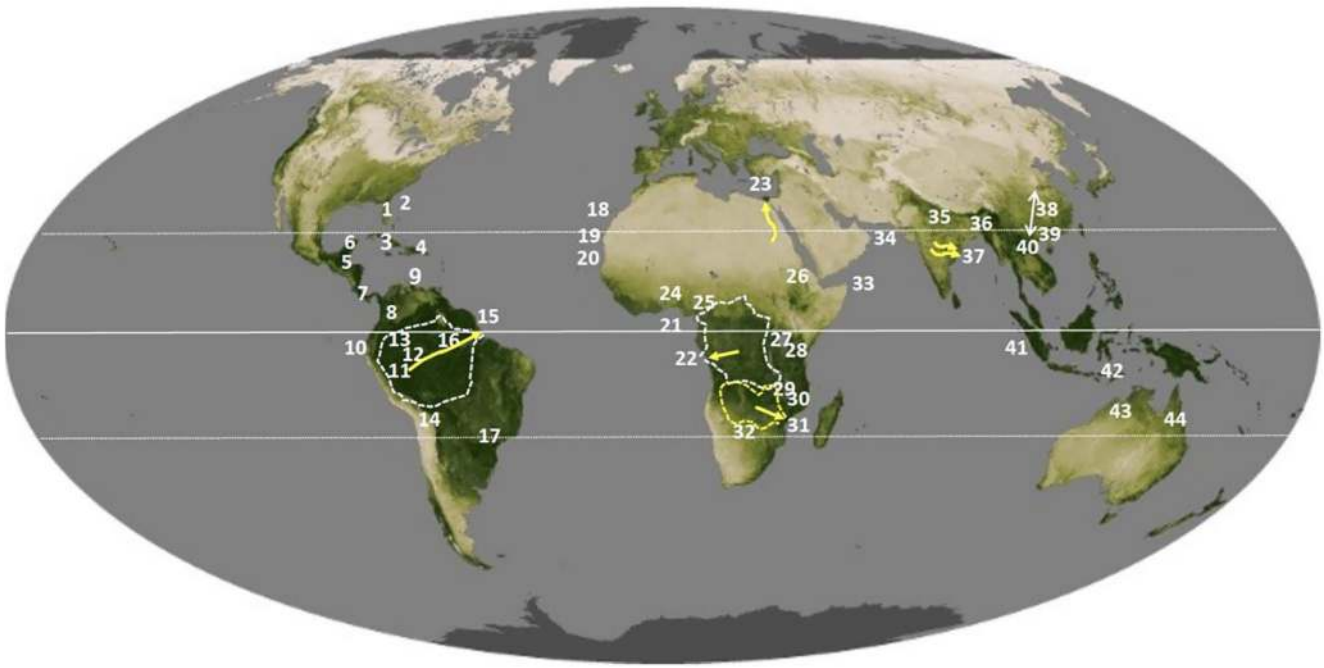

Figure 2. Locations mentioned in the text: 1. Lake Tulane, Florida; 2. Abaco Island, Bahamas; 3. SantoTomás Cave, western Cuba; 4. Larga Cave, Puerto Rico; 5. Lake Petén Itzá, Guatemala; 6. Terciopelo Cave, Nicoya Peninsula, Costa Rica; 7. Río Secreto Natural Reserve, Yucatan, Mexico; 8. Sabana de Bogotá, Colombia; 9. Cariaco Basin, Venezuela; 10. Gulf of Guyaquil, Ecuador/Perú; 11. Pacupahuain Cave, central Perúvian Andes; 12. El Condor and Diamante caves, northern Amazonian Perú; 13. Santiago Cave, Amazonian Ecuador; 14. Salar de Uyuni, Bolivia; 15. Offshore of Nordeste, Brazil; ; 16. Paixão cave, northeastern Brazil; 17. Santana and Botuverá caves, southeastern Brazil; 18. Offshore of Cape Blanc, Western Sahara/Mauretania; 19. Offshore of Senegal River, Senegal; 20. Offshore of Guinea-Bissau; 21. Gulf of Guinea; 22. Offshore of Congo River (extent of Congo Basin indicated by dashed line); 23. Offshore of the Nile River delta; 24. Lake Bosumtwi, Ghana; 25. Lakes Bambili and Barombi Mbo, Cameroon; 26. Lake Tana, Ethiopia; 27. Lake Albert, Uganda/Democratic Republic of the Congo and Lake Victoria, Uganda/Tanzania; 28. Lake Challa, Tanzania/Kenya; 29. Lake Tanganyika, Tanzania/Democratic Republic of the Congo; 30. Lake Malawi, Malawi, Mozambique; 31. Offshore of Zambezi River; 32. Makgadikgadi Basin, Botswana; 33. Moomi cave, Socotra Island, Yemen; 34. Offshore of the Indus delta, Arabian Sea; 35. Bittoo cave, northern India; 36. Mahmluh cave, Meghalaya, northwestern India; 37. Offshore of the Godavari and Mahanadi rivers, Bay of Bengal; 38. Multiple speleothems, China; 39. Huguang Maar, southern China; 40. Thuong Thien cave, northern Vietnam; 41. Offshore of Sumatra; 42. Flores, Indonesia; 43. Ball Gown Cave, northwestern Australia; 44. Lynch's crater, northeastern Australia. Dotted lines and arrows indicate major river watersheds for which offshore sediments provide proxy information. Base map shows a MODIS satellite-derived vegetation index for January 2001 (https://earthobservatory.nasa.gov/global-maps/MOD_NDVI_M).

summer/boreal winter) there is a northward transfer of atmospheric energy across the equator and when the ITCZ is in the Northern Hemisphere (boreal summer/austral winter) there is a southward transfer of atmospheric energy across the equator (Donohoe et al., 2013, 2014; Held, 2001; Schneider et al., 2014). Today, because of the oceanic transport of energy into the northern hemisphere via the AMOC, the northern hemisphere is generally warmer than the southern hemisphere and so the *mean position* of the ITCZ is slightly north of the Equator, which leads to a compensating net flux of atmospheric energy into the southern hemisphere. It follows that a reduction in the oceanic flux of energy into the northern hemisphere (due to a reduction or cessation of the AMOC, or a major change in albedo due to expansion of sea-ice–or both) would result in a southward shift in the mean position of the ITCZ, such that the *net* atmospheric energy flux would then be from the southern to the northern hemisphere. Thus, the magnitude of the overall ITCZ displacement (latitudinally) would depend on the interhemispheric temperature difference.

Figure 4 illustrates the consequences of seasonal changes in the Hadley circulation (today), in terms of (zonal mean) rainfall distribution; the convective rainfall belt is confined to a narrow belt over oceanic regions and varies little throughout the year, whereas over continental areas where large seasonal changes in surface heating occur, heavy amounts of summer rainfall extend far from the equatorial ITCZ (Figure 5). Regions with large seasonal changes in rainfall are commonly described as having a monsoon rainfall regime (Gadgil, 2018; Geen et al., 2020). Regional variations due to the distribution of the continents and seasonal changes in circulation create sharp boundaries (geographically and temporally) between areas with a high (convective) rainfall climate regime, and much drier areas where warm, subsiding air is dominant.

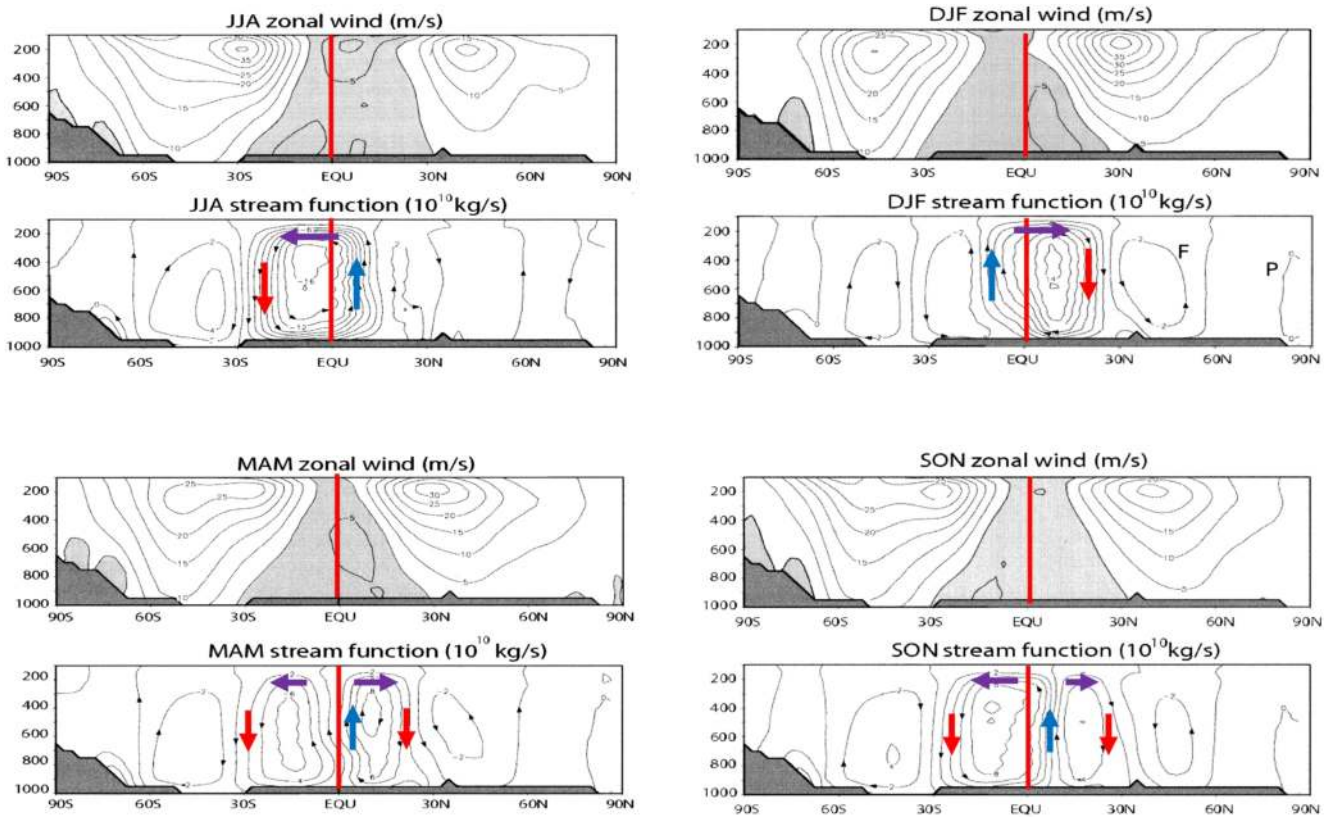

Figure 3. Zonally averaged wind (m s^{-1}) (easterly winds shaded) and mass stream function (mean flow with height and latitude) (10^{10} kg s^{-1}) for 4 seasons, shown with respect to latitude and altitude (pressure in hPa). Reprinted, with modifications, by permission from Springer: *The Hadley Circulation: Present, Past and Future* (eds. H.F. Diaz and R.S. Bradley), Webster, P.J., The elementary Hadley circulation, 9–60, ©2013.

The distribution of rainfall during the northern (or southern) summer months, when surface heating is greatest, is influenced by the extent of land areas, topography and other factors in each continental region (cf. Atwood et al., 2020; Mamalakis et al., 2021), as well as the specific humidity of air entering into convective plumes which transfer moist static energy aloft. The delivery of moist air masses to continental interiors (via the Trade winds and monsoonal systems) is closely linked to upwind sea surface temperatures and wind strength. The distribution and amount of rainfall therefore depends on a combination of large-scale circulation dynamics (the Hadley circulation) and local thermodynamics (available moist static energy), which varies regionally (Schneider et al., 2014). For example, in the Americas, convective rainfall extends far southward across the Amazon lowlands in January (austral summer), with moist air transported inland via the northeast Trade winds, while the Pacific coastal margins remain dry due to the topographic barrier of the Andes (which limits moisture flux from the east) and the cool oceanic current offshore, where convection is suppressed (Garreaud et al., 2009). During boreal summer, Amazonia is relatively dry as the zone of maximum rainfall shifts toward Central America, but due to the more limited land mass there, the seasonal displacement to the north is less pronounced. Over Africa, the geography is quite different with an extensive landmass extending across the tropics and sub-tropics, and highlands across much of East Africa. The zone of deepest convection and maximum rainfall occurs south of the zone of surface wind convergence, with the heaviest rainfall in Equatorial Africa caused by mesoscale convective systems that develop over the East African Highlands (Nicholson, 2018) and topographically controlled low-level jets delivering moisture into the African interior from the Indian Ocean (Munday et al., 2021).

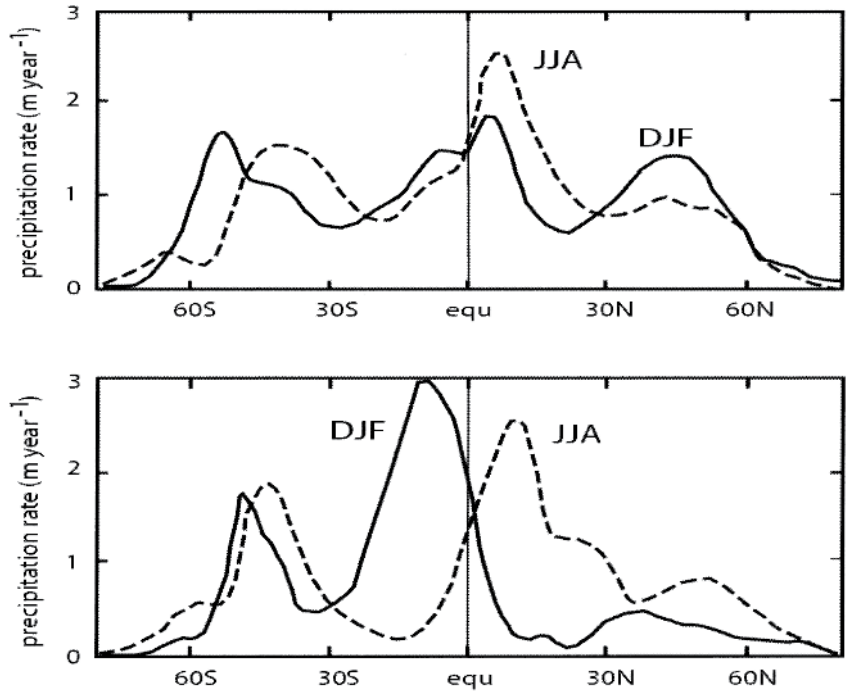

Figure 4. Zonal mean rainfall distribution over the oceans (above) and over continental regions (below). Reprinted by permission from Springer: *The Hadley Circulation: Present, Past, and Future* (eds. H.F. Diaz and R.S. Bradley), Webster, P.J., The elementary Hadley circulation, 9–60, ©2013.

3. The Signal of THEs in the Americas

3.1. Florida, the Bahamas and the Caribbean

In Florida, lower sea-level and generally drier conditions led to lower water tables during the last (Wisconsin) glaciation, so only the deepest lakes had continuous sedimentary records from that period (Watts & Hansen,, 1994). Lake Tulane, in south-central Florida is one example: an 18.5 m core spans the last ~50–60,000 calendar years (though dating of the record before ~40 ka is somewhat problematical; Grimm et al., 2006). The pollen record from this site shows pronounced oscillations in the percentage of *Pinus* (pine) pollen, which varies in opposition to the percentages of *Quercus* (oak) and *Ambrosia* (ragweed and marsh-elder). This is interpreted as a shift from pine to oak-savanna or open grassland-type vegetation, with abrupt transitions between the two (Grimm et al., 1993, 2006). These changes represent a shift in moisture availability, with the pine phase resulting from warm, wet intervals separated by drier episodes when oak dominated the landscape and the lake level was lower. Periods of pine abundance (named "TP1" to "TP6") were correlated with HEs HE1 to HE6 (within fairly large dating uncertainties), though the pine expansion associated with HEs HE2 to HE4 lasted longer, starting before and continuing after the corresponding HEs. van Beynen et al. (2017) also found evidence for warmer and wetter conditions (relative to the prevailing glacial climate) around the time of HE 2 in a stalagmite from northwestern Florida. Grimm et al. (2006) interpreted these changes as due to a reduction in northward flowing tropical water into the North Atlantic (due to a slowdown in the AMOC), which resulted in warming of the Gulf of Mexico and the Caribbean Sea, and the adjacent land areas (cf. Rühlemann et al., 1999). In addition, a wider (more continental) Florida peninsula when sea level was lower may have led to more convective summer rainfall. Thus, conditions in south-central Florida were relatively wet and warm (year-round) during HEs (Arnold et al., 2018; Grimm et al., 2006).

This record stands in contrast to conditions just east of the Florida peninsula, in the Bahamas, and to the south in Cuba and Puerto Rico. A stalagmite record from Abaco Island in the Bahamas provides strong evidence that sea surface temperatures during HEs 1–3 averaged ~4.3°C ± 2.7°C cooler than present, with oxygen isotopic maxima at ~15, 24.1, and 31.5 ka B.P. (Arienzo et al., 2017, 2015). SSTs were particularly cool

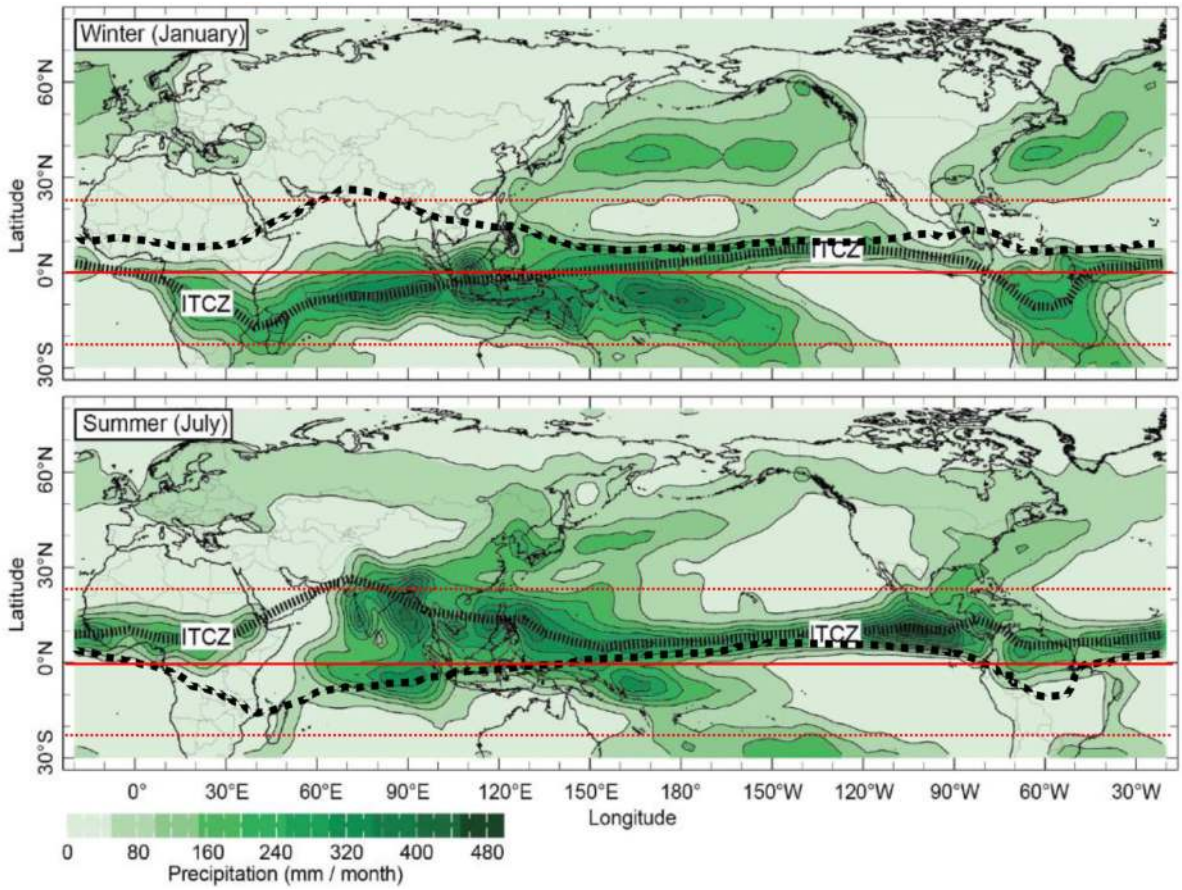

Figure 5. January and July (boreal winter and summer) rainfall totals and position of the ITCZ; black dotted lines indicate the ITCZ location in the opposing season. Red lines denote the Equator and Tropics of Cancer and Capricorn. Reprinted, with modifications, by permission from Springer: *Nature Geoscience*, 6 (3), Deplazes, G., Lückge, A., Peterson, L.C., Timmermann, A., Hamann, Y., Hughen, K.A., Röhl, U., Laj, C., Cane, M.A., Sigman, D.M., Haug, G.H., Links between tropical rainfall and North Atlantic climate during the last glacial period. 213–217. ©2013.

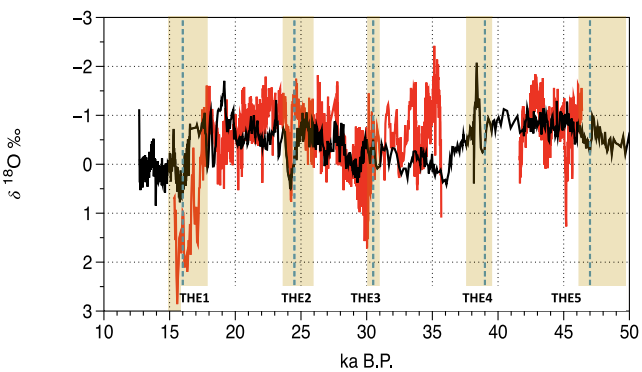

Figure 6. Oxygen isotope record from stalagmites in Santo Tomas Cave, Cuba (black) and Cueva Larga, Puerto Rico (red; Warken et al., 2019, 2020). Dashed blue lines indicate the timing of maximum IRD in the stacked record of 15 North Atlantic cores (from Lisiecki & Stern, 2016). Shaded brown intervals indicate times when IRD exceeded median values for MIS2–4. **Data sources:** https://doi.org/10.1594/PANGAEA.911486; https://doi.pangaea.de/10.1594/PANGAEA.912646.

(by ~5.9°C) in HE1. Fluid inclusions within the stalagmite indicate that precipitation amounts were not significantly different from today during those intervals. These SST estimates are similar in magnitude to those derived for HEs 4 and 5, from alkenones in sediments from the Bermuda Rise (Sachs & Lehman, 1999), indicating a significant change in the position and/or temperature of the Gulf Stream during HEs. It is noteworthy that bathymetric data from off the Atlantic coast of Florida reveal iceberg scours as far south as the Florida Keys (~24°N), most dating from HE3 (Condron & Hill, 2021; Hill & Condron, 2014). High-resolution model simulations indicate that cold water from the Labrador Sea could have transported icebergs within a narrow southward-flowing coastal current, and this may explain why temperatures were cooler in the Bahamas during Heinrich episodes, while relatively warm waters were found further west, within the Gulf of Mexico. A speleothem record from Cuba, spanning the last ~96 ka, also suggests that generally cooler and drier conditions prevailed during HEs, as recorded by a reduction in growth rates and a slight enrichment in oxygen isotopes (Warken et al., 2019). This conclusion is reinforced by trace element and $\delta^{18}O$ in a stalagmite from Larga Cave, Puerto Rico, which registered consistently dry conditions during the time of HEs 1–4 (Warken et al., 2020; Figure 6).

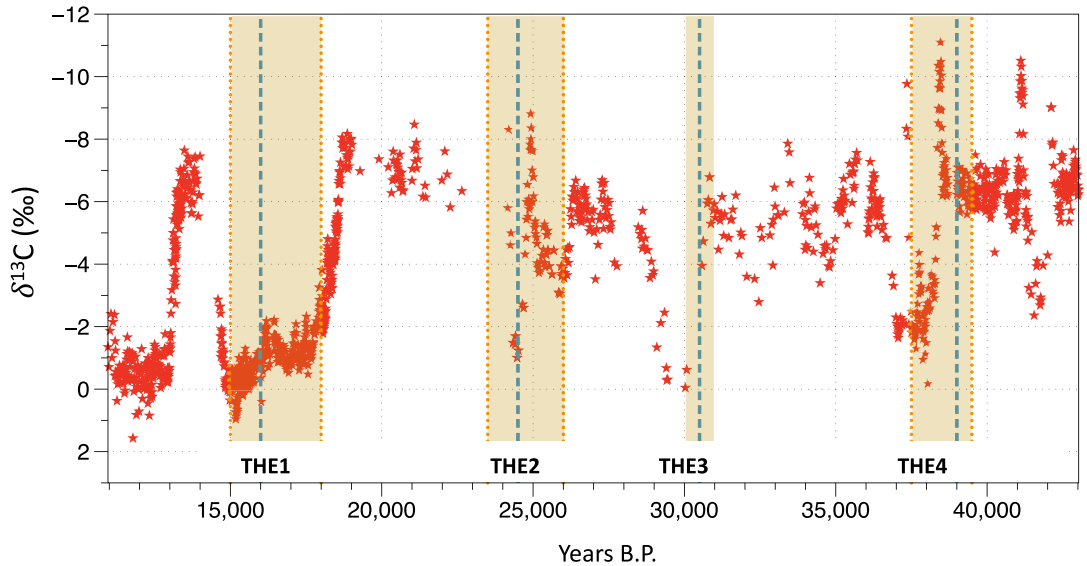

Figure 7. Carbon isotope data from Lake Petén Itzá, Guatemala, based on the ostracod *Lymnocythere opesta* in core PI-6 (chronology updated [pers. comm., J. Escobar & M. Brenner]; isotopic data from Escobar et al., 2012). Dashed blue lines indicate the timing of maximum IRD in the stacked record of 15 North Atlantic cores (from Lisiecki & Stern, 2016). Shaded brown intervals indicate times when IRD exceeded median values for MIS2–4.

3.2. Central America

The longest terrestrial record from Central America is from Lake Petén Itzá, a closed basin lake in the lowlands of northern Guatemala where a sediment core (PI-6) spanning the last ~75 ka was recovered (D. Hodell, *pers. comm.*, 2021). The climate at this latitude (~17°N) is subtropical (mean annual temperature of ~25°C) with a strong seasonal cycle of rainfall related to the northward migration of the ITCZ in summer months, when convective activity increases, but much drier conditions due to enhanced subsidence, when the ITCZ moves southward in winter months (Hodell, Anselmetti, et al., 2008). The sediments in Lake Petén Itzá consist of an alternation of distinct units, varying from clay-rich facies, deposited during wetter intervals, to beds with a high concentration of gypsum, deposited during dry periods when lake volume declined and lake water salinity increased. These changes are reflected in the magnetic susceptibility of the sediments, with the lowest values during the driest intervals. Changes in water chemistry associated with lake level fluctuations are also recorded in the $\delta^{13}C$ and $\delta^{18}O$ of ostracods in the sediments. Higher values of both isotopes occur when lake levels were low and the coring site was within the well-mixed epilimnion (and/or warmer conditions prevailed; Escobar et al., 2012). An alternative explanation is that changes in ostracod ^{13}C resulted from changes in pore water caused by the input of terrestrial organic carbon, which had switched from C3 to predominantly C4 vegetation during dry intervals (Mays et al., 2017). Evidence from ostracod assemblages suggests that water temperatures were <3°C lower during MIS2–4 (Cohuo et al., 2018) whereas palynological evidence suggests that air temperatures were cooler (by ~5°C–7°C) during the Last Glacial Maximum (LGM, centered at 21 ka B.P.). However, the no-analog vegetation assemblage which was present at that time makes such estimates quite uncertain (Bush & Colinvaux, 1990; Correa-Metrio et al., 2012a, 2012b). Clumped isotope thermometry and gypsum hydration water indicate conditions may have been even cooler (−5°C to −10°C relative to the Holocene average;Grauel et al., 2016; Hodell et al., 2012). With the cooling of that magnitude, evaporation from the lake (and the watershed) would have been diminished, but the lowest lake levels (as much as 56 m below present day) occurred before and after the LGM, as indicated by both lithological and isotopic evidence, so rainfall amounts must also have been significantly reduced (Correa-Metrio et al., 2012b). Lake Petén Itzá is ideally situated, and deep enough to have recorded such large hydroclimatic changes. Most importantly, the timing of each episode of gypsum deposition, and high values of $\delta^{13}C$ and $\delta^{18}O$ roughly corresponds to a HE in the North Atlantic (Figure 7). Hodell, Anselmetti, et al. (2008) argued that these dry intervals reflect a southward shift in the mean position of the ITCZ over Central America, resulting in very little convective rainfall in summer and thus a

significant decline in lake water volume. There may also have been less convective rainfall within the ITCZ as a result of cooler Atlantic SSTs, leading to less moisture flux to the convergence zone as well as a reduction in the number and intensity of tropical depressions from the sub-tropical Atlantic (Escobar et al., 2012; Medina-Elizalde et al., 2017; Stager et al., 2011). During the LGM *sensu stricto*, cold season precipitation associated with frontal systems from North America (*Nortes*) may have compensated somewhat for the lower summer rainfall amounts (Bush et al., 2009). Lower lake levels during THEs are clearly seen in $\delta^{13}C$, reflecting oxygenation of the entire water column at those times, and in magnetic susceptibility, recording the precipitation of gypsum from the water column. However, evidence from ostracods and diatoms (indicative of water conductivity) indicate that not all THEs were similar. Although all THEs resulted in high species variability as the water level fell and habitats within the lake were drastically altered, THEs 1 and 5 appear to have been the most extreme (coldest and driest). In contrast, THEs 5a and 6 were relatively warm, though still quite dry (Perez et al., 2021).

Also of note is the rapid alternation of sediment facies within THE1, shifting from gypsum to a thin clay-rich layer and back again to gypsum, indicating that a brief interval of fluvial discharge punctuated the otherwise very dry period. This is also recorded as a rapid alternation in $\delta^{18}O$ and (to a lesser extent) in $\delta^{13}C$. As discussed later, such rapid alternations in hydroclimatic conditions have also been noted in other locations, and for other THEs.

Evidence for abrupt hydroclimatic (THEs) around the time of North Atlantic HEs is also found in stalagmites from the Pacific coast of Costa Rica, although the magnitude of such effects varies. During HE6 and HE2 rainfall was particularly low, consistent with prolonged displacement of the ITCZ, but the signal for drier conditions is not so evident during other HEs, perhaps because of Pacific influences on local rainfall in that region (Lachniet et al., 2009). An exceptionally high-resolution stalagmite record from Yucatán, Mexico spans the time interval of HE2 and reveals an overall 50% reduction of rainfall during this period, within which were a series of short-term even drier episodes (Medina-Elizalde et al., 2017). The authors suggest that such dry conditions (across the wider Caribbean and Gulf of Mexico) may have led to more saline oceanic conditions feeding into the Gulf Stream, potentially leading to a resumption in strength of the AMOC.

3.3. Colombia

The longest and most detailed pollen record from the Americas comes from the montane basin of the Sabana de Bogotá in Colombia (~5.5°N), where a subsiding basin has preserved a record of environmental changes spanning the Quaternary (Hooghiemstra, 1984; Torres et al., 2013). Vegetation in the area is zoned altitudinally, ranging from tropical forest below ~1,000 m, to Andean forest above ~2,300 m, to páramo above ~3,500 m. At the highest elevations, perennial snow is found. Pollen has been analyzed throughout the period of record, but in remarkable detail (~60 yr resolution) for the last 284 ka resulting in one of the most detailed paleoclimatic reconstructions from the tropics (Groot et al., 2011, 2013). The main focus of most studies has been changes in temperature that are reflected in the percentage of arboreal pollen (AP%), which is strongly correlated with temperature-driven changes in the upper forest limit. Regional studies indicate that a 10% change in AP% corresponds to a change in mean annual temperature of 1.3°C ± 0.3°C (assuming a steeper lapse rate during glacial times; Wille et al., 2001). Over the last 284 ka, AP% has varied from ~10% to >90%, indicating that temperatures at Lake Fuquene (in the eastern cordillera of Colombia, around 2,500 m) varied from ~6°C during glacial maximum conditions to ~17°C at the peak of interglacial warmth. Over the long-term, orbital forcing was the primary factor affecting vegetation changes (driven by related changes in ice sheet growth and the migration of the ITCZ) but millennial-scale changes are also apparent, with rapid changes in forest composition that appear to be associated with DO events in the North Atlantic (Groot et al., 2011). The pollen data are more difficult to quantify in terms of hydroclimate, but during HE1 and HE3-HE6, the area was relatively wet. During HE2, the evidence is less clear; it was certainly colder but may also have been relatively dry in some parts of the country where the complex topography makes it difficult to define the overall regional patterns of hydroclimatic changes (Groot et al., 2013; Patiño et al., 2020; Velásquez-R & Hooghiemstra, 2013).

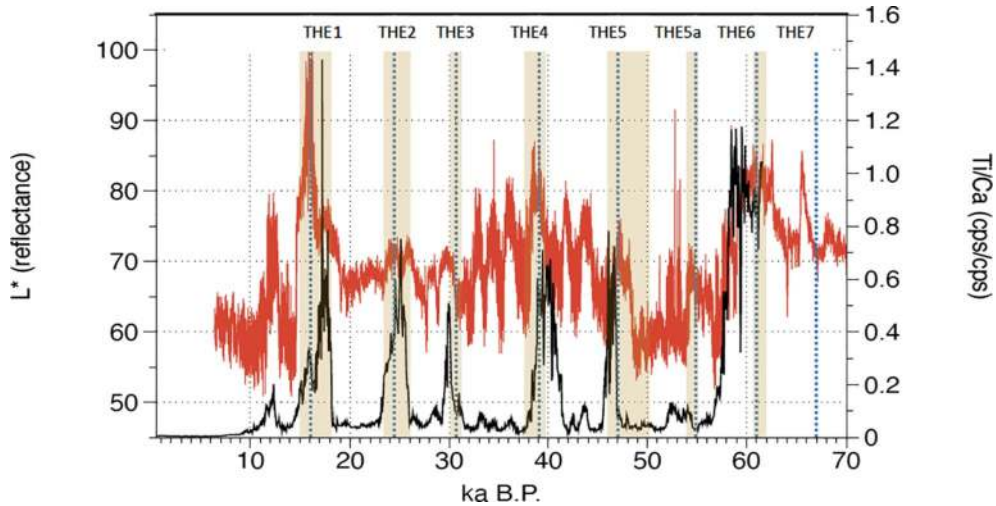

Figure 8. Reflectance (L*) in a sediment core from Cariaco Basin (core MD03-2621; 10.7°N, 65°W) (from Deplazes et al., 2013) [in red] and Ti/Ca ratios from a core off NE Brazil (GeoB 3910-2; 4.2°S; 36.3°W) (Jaeschke et al., 2007) [in black]. THEs 1–6 are clearly seen, as well as minor anomalies during the Younger Dryas chron and at ~55 ka B.P. Dashed blue lines indicate the timing of maximum IRD in the stacked record of 15 North Atlantic cores (from Lisiecki & Stern, 2016). Shaded brown intervals indicate times when IRD exceeded median values for MIS2–4. Data sources: https://doi.org/10.1594/PANGAEA.815882 (Cariaco Basin); https://doi.org/10.1594/PANGAEA.667497 (GeoB 3910-2, Ti/Ca).

3.4. Northern South America: Cariaco Basin

In the Cariaco Basin, off the coast of Venezuela, anoxic conditions result from high surface productivity and a restricted circulation due to a shallow sill, which separates the basin from the open ocean. This unusual condition leads to the preservation of sediments with minimal bioturbation (and at times annual laminations) at depths below 300 m, alternating between light-colored, foram and silica-rich sediments, and darker sediments rich in organic carbon (Peterson et al., 2000, 1991). These different facies reflect large-scale circulation changes. When the ITCZ migrates far to the south, northeasterly Trade winds lead to an upwelling of cool nutrient-rich waters; as the ITCZ migrates northward, heavy convective rainfall leads to a surge in runoff from rivers draining into the Caribbean from the northern coast of South America, with an increase in minerogenic material and organic carbon from the continent. Changes in the dominant mode of deposition can be seen in the total color reflectance ("lightness," L*), which therefore provides an index of the prevailing circulation regime, and the relative position of the ITCZ in the region (Deplazes et al., 2013; Figure 8). The Cariaco Basin reflectance (L*) record is highly correlated with isotopic changes in Greenland on the millennial timescale, with most of the DO events recorded by sedimentary changes (Hughen & Heaton, 2020). Periods of foram-rich reflective sediments are also apparent at the time of certain HEs, such as HE1 and HEs 4–7. By analogy with the seasonal changes in sediment deposition today, these events were associated with strong upwelling (persistent Trade winds) when the ITCZ was displaced far enough to the South that there was minimal runoff and limited minerogenic sediment flux from the adjacent continent. However, there are several other periods with similar reflectance anomalies that were not associated with known HEs. Another parameter that provides a strong record of terrestrial sediment input to the Cariaco Basin is elemental Fe, which shows distinctly low values during HEs HE3 to HE6, indicating little runoff from South America at those times and thus low rainfall amounts over the river catchments that drain into the Caribbean (Jaeschke et al., 2007).

3.5. Ecuador and Peru

Sediment cores from off the coast of northern Peru (at ~4°S, in the Gulf of Guyaquil) provide a record of terrestrial runoff spanning the last ~18 ky (Mollier-Vogel et al., 2013). Ti/Ca elemental ratios reflect dilution of the carbonate fraction due to high amounts of sediment transported into coastal waters. Increased sediment flux occurred during THE1 (~14–18 ka B.P.), with a minor increase also during the Younger Dryas chron.

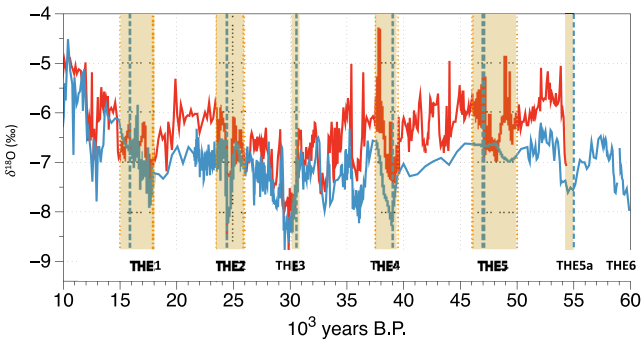

Figure 9. Stalagmite $\delta^{18}O$ records from Cueva del Diamante (blue) & El Condor (red) caves in the Peruvian Amazon Basin (modified from Cheng et al., 2013). Data source: https://www.ncdc.noaa.gov/paleo-search/study/20450.

This is opposite to the changes recorded in Central America, where the driest conditions of the last 85 ka were recorded during THE1. In the Andes of central Perú (~11°S) cave stalagmites record generally higher rainfall (a stronger South American monsoon) at the time of HEs (particularly HE3 and HE4) though the signal is complicated by considerable millennial-scale variability linked to DO events (Kanner et al., 2012). Further east, on the Amazonian side of the Andes (at ~6°S) stalagmites also record higher rainfall at the time of most North Atlantic HEs. As in central Perú, the most isotopically light values of (at least) the last 60,000 yr occurred during the time of HE3, despite reduced insolation due to orbital (precessional) forcing (Figure 9; Cheng et al., 2013). Furthermore, it is likely that precipitation was also relatively enriched during glacial time, due to isotopic changes in the glacial ocean and lower temperatures (Kanner et al., 2012; Mosblech et al., 2012), so the isotopic shift recorded during THE3 may, in a sense, underestimate the magnitude of change in precipitation, relative to earlier events when ice sheets were smaller and cooling was probably less. Stalagmites from closer to the Equator, in the Ecuadorian Amazon at ~3°S, registered isotopically depleted rainfall around the times of most Heinrich episodes, but THE3 was not strongly recorded. Whether this was an artifact of the particular sample or a true reflection of conditions close to the Equator at that times is unclear, as there were significant hydroclimatic anomalies around the time of all other HEs (Figure 10; Mosblech et al., 2012). Despite this one anomaly, collectively these records show that, to the south of the Equator, the dominant hydroclimatic signal at the time of North Atlantic HEs switched from the droughts found further north, to much higher than average rainfall amounts. Interestingly, there were significant centennial-scale changes in runoff to the Gulf of Guayaquil during the most recent THE1, which correspond in time to changes in monsoon rainfall recorded by speleothems in China (H. Zhang et al., 2019). However, these fluctuations are of opposite sign in China, with wetter (isotopically lighter) conditions there, when runoff from the coast of southern Ecuador was reduced. There are few other records with sufficient resolution to detect such changes, though it is clear that THE1 was also not a monotonic event at Lake Petén Itzá, or in the Cariaco Basin, or the Arabian Sea (Deplazes et al., 2013, 2014; Escobar et al., 2012). Furthermore, the stalagmites from central Peru also show similar centennial fluctuations during THE4 and THE5, suggesting that such variations may be more widespread and common during North Atlantic HEs (Kanner et al., 2012).

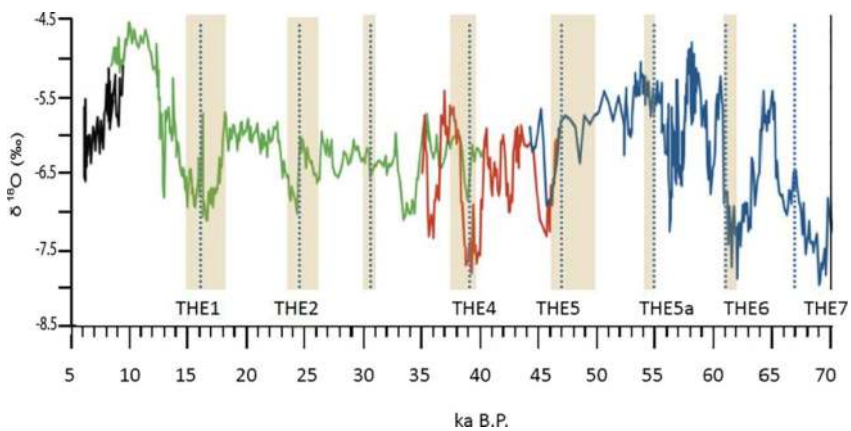

Figure 10. Composite oxygen isotope record in 4 stalagmites (shown by different colors) from Santiago Cave, eastern Ecuador. More negative values indicate wetter conditions. Times of peak IRD in a stacked record from the North Atlantic are shown by the blue lines (cf. Figure 1; from Mosblech et al., 2012, Supplemental). Dashed blue lines indicate the timing of maximum IRD in the stacked record of 15 North Atlantic cores (from Lisiecki & Stern, 2016). Shaded brown intervals indicate times when IRD exceeded median values for MIS2–4. Data source: https://www.ncdc.noaa.gov/paleo-search/study/13733.

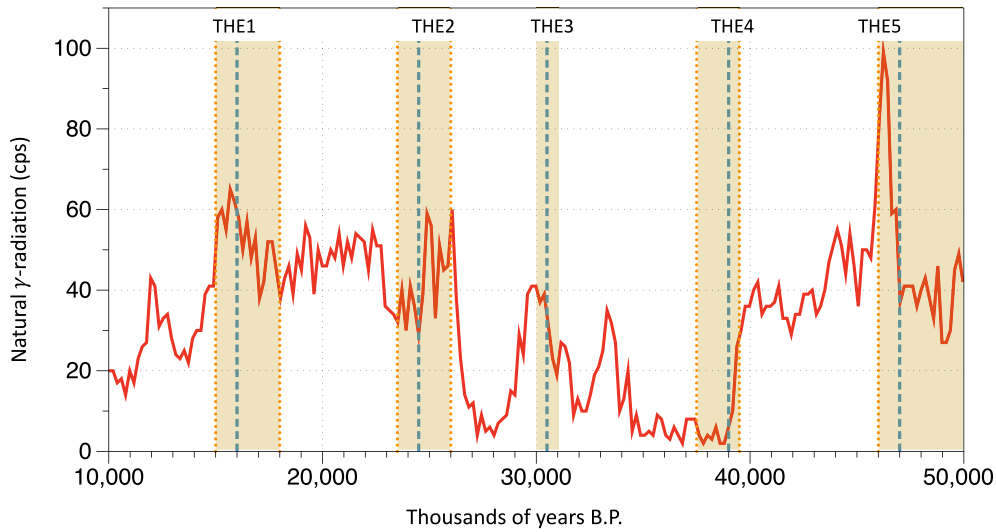

Figure 11. Natural gamma radiation, a proxy for effective moisture, in a sediment core from Salar de Uyuni, Bolivia (from Baker et al., 2001). The gamma radiation is a result of the radioactive decay of K, U, and Th, elements that are more concentrated in the lacustrine muds than in salt deposits; hence higher values are indicative of wetter conditions. Millennial-scale increases in rainfall are superimposed on low-frequency changes driven by precessional forcing. A volcanic ash at ~45,000 yr B.P. contributed to the exceptionally high values of gamma radiation at that time. Paleolake Tauca reached its maximum size at ~16,000 yr B.P., more than doubling the area of the Salar de Uyuni (Blard et al., 2011). Dashed blue lines indicate the timing of maximum IRD in the stacked record of 15 North Atlantic cores (from Lisiecki & Stern, 2016). Shaded brown intervals indicate times when IRD exceeded median values for MIS2–4. Data source: https://www.ncdc.noaa.gov/paleo-search/study/9952.

3.6. Bolivia

Several periods of major lake expansion and contraction have occurred on the Bolivian Altiplano (Baker et al., 2001; Placzek et al., 2013). Paleolake Tauca (15°–22°S) reached its maximum size (52,000 km^2, almost as large as Lake Michigan) from 14.5 to 16 ka B.P., as recorded by shoreline features and diatom-rich mud facies, in sediment cores recovered from what is now an extensive salt flat (Salar de Uyuni; Baker et al., 2001; Blard et al., 2011). Isotopic data from the Sajama ice core (Thompson et al., 2000) indicate that snowfall was relatively enriched at that time, most likely reflecting this local moisture source adjacent to the ice cap. The timing of earlier wet phases is less certain, but similar mud layers appear to correspond to the timing of HE2, HE3, HE4 and possibly, HE5 (Figure 11). Although there may have been changes in river systems linking the various Altiplano drainage basins, hydroclimate model simulations suggest that, even with temperatures 5°C lower, precipitation must have increased by at least 350 mm/yr (2–3 times modern values) to maintain a lake the size of paleolake Tauca (Nunnery, 2012). Thus, periods of lake expansion resulted from much wetter conditions associated with a southward shift in the zone of maximum summer rainfall, as seen in records from Perú.

3.7. Brazil

Sedimentary records from off the coast of northeastern Brazil (Nordeste, from ~0°–3.7°S) provided the first indication that pronounced hydrological changes on the continent were associated with HEs (Arz et al., 1998, 1999; Behling et al., 2000; Jaeschke et al., 2007; Jennerjahn et al., 2004; Nace et al., 2014). Increased chemical weathering during wet periods in the tropics leads to higher levels of iron relative to potassium in detrital sediments eroded from the landscape. Similarly, the flux of titanium from the continent, relative to pelagic carbonates (assumed to be constant) also provides an index (Ti/Ca) of precipitation amount and river runoff. Pulses of Fe and Ti-rich sediments are clearly synchronous with HEs 1–9 (Figure 12), indicating periods of high runoff from Nordeste rivers. At the same time that these indices reveal higher levels of precipitation, Mg/Ca ratios of isotopically light planktonic forams indicate slightly higher SSTs and lower salinities offshore (Nace et al., 2014). These changes all point to stronger convective rainfall

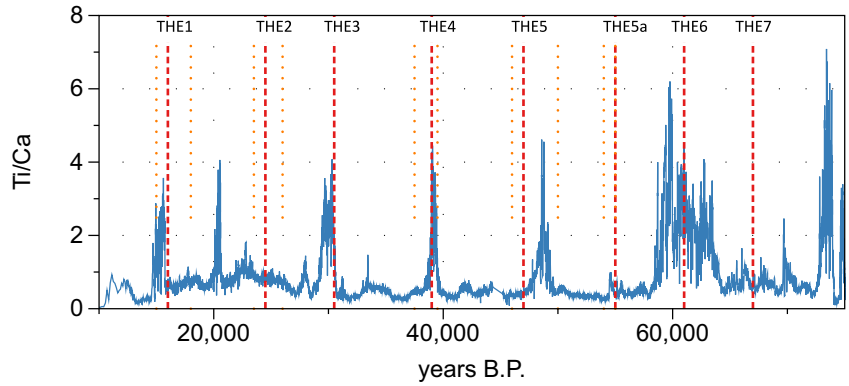

Figure 12. Ti/Ca ratio for marine sediment core CDH 86, off the mouth of the Amazon River (0.3°N, 44° 12.2°W). The Ca is derived from biogenic $CaCO_3$ (mostly from pteropods, foraminifera, and calcareous nannoplankton) which is assumed to have been relatively constant over time. High ratios thus indicate that higher amounts of clastic material were delivered to the ocean during times of relatively wet conditions in the continental interior (adapted from Nace et al., 2014). Red lines denote peak times of IRD (from Figure 1).

in the Nordeste region during HEs, as a result of a more persistent ITCZ over the region, which is an expected consequence of colder conditions in the northern hemisphere (Chiang & Friedman, 2012). At the same time, warm SSTs in the Atlantic south of the Equator and stronger Southeast Trade winds may have increased moisture flux to the continent. A slowdown in the AMOC would have led to a reduction in the flux of heat northward in the North Brazil Current and the accumulation of relatively warm water offshore (Arz et al., 1999). It is interesting to note that, for THE1 at least, pollen data in offshore sediment cores indicate there was a two-phase increase in Nordeste rainfall. From ~18 ka to 16.5 ka B.P., rainfall increased enough to support gallery forests along rivers and streams, but from 16.5 to 15 ka B.P., there was more widespread rainforest vegetation with tree ferns, suggesting year-round humid conditions (Dupont et al., 2010). Oxygen isotope data from Paixão cave stalagmites in northeastern Brazil also indicate that there were two distinct periods when rainfall increased, from 18.1 to 16.66 ka B.P. and from~16.1 to 14.69 ka B.P. (when rainfall reached its maximum) before declining again by the beginning of the Bølling-Allerød interstadial (Stríkis et al., 2015). It is noteworthy that this later period precisely corresponds to the time of an abrupt increase in CH_4, thought to be from southern hemisphere tropical wetlands, as recorded in a West Antarctic ice core (Rhodes et al., 2015). A two-step pattern is also seen during THE4 and THE5 in the stalagmite records from central Perú (Kanner et al., 2012). Wetter conditions were also recorded in caves from northeastern and central-eastern Brazil at other times, with rainfall maxima centered at ~39.2, 48.2, and 60.5 ka B.P., close to the timing of HEs 4, 5, and 6 (Stríkis et al., 2018). Similarly, stalagmites from the western Amazon Basin registered higher rainfall at those times, as well as at ~24 and ~30 ka B.P., corresponding to HEs 2 and 3 (Cheng et al., 2013). Wetter conditions during HEs were also clearly recorded further south in eastern Brazil (~10°S) by periods of stalagmite growth in caves that were simply too dry for such calcite deposition at other times (X. Wang et al., 2004). Isotopically depleted rainfall from the Amazon Basin even reached the southernmost parts of Brazil (~27°S) during HEs, as recorded by isotopically light $\delta^{18}O$ in stalagmite carbonate (Cruz et al., 2006, 2009; X. Wang et al., 2006). This was due to the extreme southward displacement of the ITCZ and associated convective rainfall as well as a strengthened South Atlantic Convergence Zone at those times (Stríkis et al., 2015).

4. The Signal of THEs in Africa

Sediment cores from offshore provide insight into conditions on the adjacent continent, especially near the mouths of major rivers where sediments may integrate the paleoclimatic signal from across an entire drainage basin inland. In a core from the northwestern African coast off Cape Blanc (~21°N) Tjallingii et al. (2008) used variations in grain size to distinguish between the relative flux of Saharan dust and finer-grained hemi-pelagic mud, derived from coastal rivers. This showed that there were numerous times in the past 120,000 yr when abrupt increases in the flux of aeolian sediment occurred, generally associated with minima in benthic foraminiferal $\delta^{13}C$, indicative of a reduction in deep water ventilation in the North

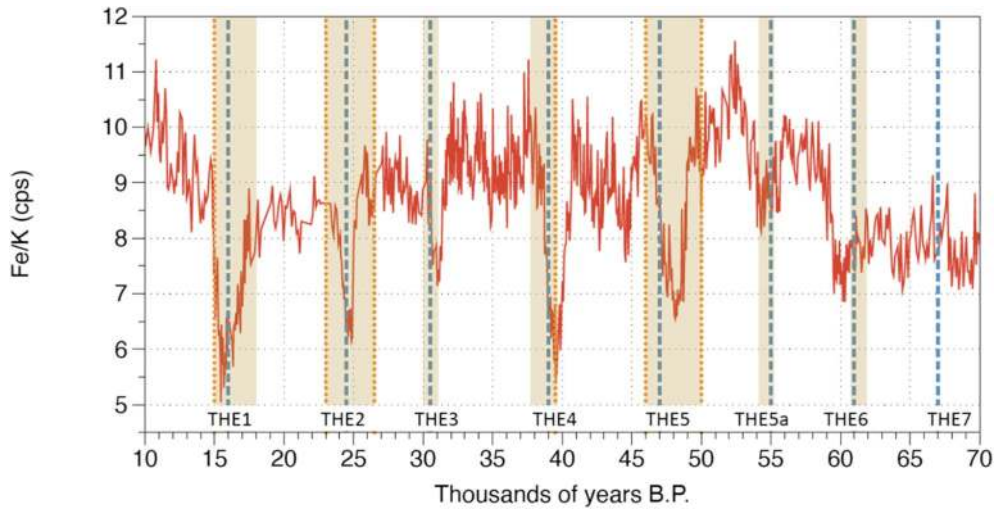

Figure 13. Ratios of Fe/K in a sediment core from off the coast of Guinea-Bissau (~12.5°N). Higher values of Fe/K indicate wetter conditions as the more weathered rocks in humid tropical regions contain more Fe relative to the more mobile potassium. The low values that punctuate this record thus indicate much drier conditions in the continental interior as the ITCZ and associated rain belt shifted southward and Trade winds delivered dust from the arid interior of the Western Sahara. Gray shading denotes the timing of Heinrich events in the North Atlantic (modified, from Zarriess et al., 2011). *Data sources:* https://doi.org/10.1594/PANGAEA.756401; https://doi.org/10.1594/PANGAEA.756437.

Atlantic (cf. Gallego-Torres et al., 2014). These abrupt THEs (which occurred within all of the last 5 marine isotope stages) were superimposed on a background of lower frequency precessional variations. Further south (at ~15.5°N), Mulitza et al. (2008) and Niedermeyer et al. (2010) analyzed sediments from core GeoB 9508 off the Senegal River. As off Cape Blanc, sediments from river outflow are fine-grained, with relatively high Fe/K and Al/Si geochemical signatures, whereas aeolian material from the Sahel is coarser and has lower Fe/K values. Changes in these ratios and grain size over the last 57,000 yr reveal five THEs with drier conditions and limited discharge from the Senegal River, which correspond to Heinrich episodes HE1 to HE5. The Younger Dryas was also drier, though not as dry as during the earlier intervals. Similarly, Zarreiss et al. (2011) analyzed Fe/K in a core from 12.5°N, off Guinea-Bissau, which clearly records drier episodes when the ITCZ and associated rain belt was displaced to the south, and dust from the arid continental interior was carried offshore (Figure 13). There is pollen evidence that the Heinrich 1 interval involved three phases, with two periods of strengthened Northeast Trade winds and increased aridity (especially the second phase) separated by a period of less severe aridity from 17.4 to 16.2 kyr B.P. (Bouimetarhan et al., 2012). This is similar to the pattern seen in a sediment core from the North Atlantic in which Hodell et al. (2017) identified two distinct episodes of ice-rafting, which they dated as occurring from 17.1 to 15.5 kyr B.P. (HE1.1) and from 15.9 to 14.3 kyr B.P. (HE1.2; see also Huang et al., 2019).

In other sediment cores, from as far south as ~12°N, Collins et al. (2013), Itambi et al. (2009), Jullien et al. (2007), and Just et al. (2012) also found strong evidence for enhanced aeolian sediment deposition during Heinrich intervals. During HE1, dust flux at 13.5°N was 80 times that of the late Holocene (Just et al., 2012) and sand dunes migrated as far south as ~14°N in Senegal, ~600 km further south than the current limit of active dunefields in the western Sahara (Collins et al., 2013). Dust and major element variations in a transect of cores from ~21°N to 9°N spanning the last ~60,000 yr, indicate that the Sahara-Sahel boundary was at ~15°N during the LGM (compared to ~19°N today), but was displaced even further southward, to ~13°N, during Heinrich intervals 1, 2, 4, and 5 (there was no strong signal of a southward shift during Heinrich 3; Collins et al. (2013). Higher values of δD in leaf wax n-C_{31} alkanes also indicate that convective rainfall in summer was reduced (and/or evaporation increased) during these intervals (Niedermeyer et al., 2010).

Moving further south along the coast into the Gulf of Guinea, $\delta^{18}O$ in forams record changes in sea surface salinity, which is affected by variations in river flow and the isotopic composition of rainfall (Weldeab, 2012; Weldeab et al., 2007). More enriched isotopic values are clearly seen during North Atlantic Heinrich

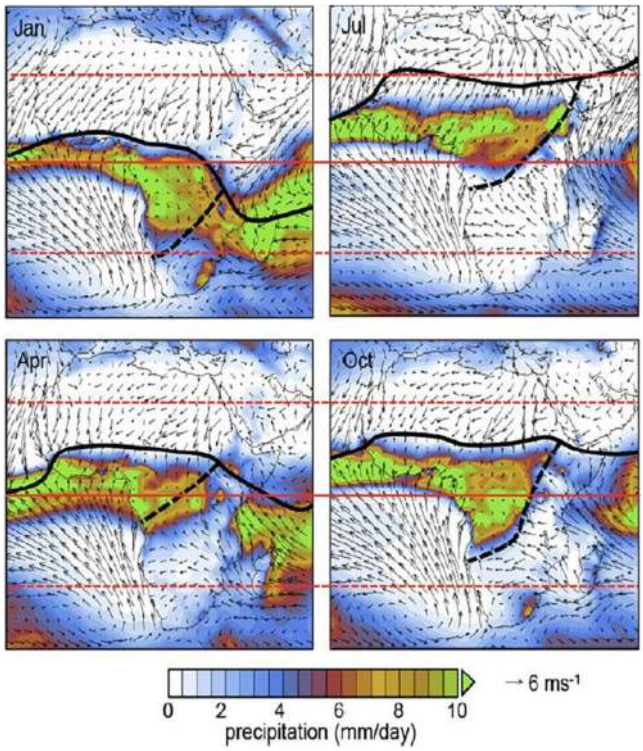

Figure 14. Monthly mean precipitation in mm/day (filled contours) and 10 m winds from ERA Interim re-analysis (1979–2013 average). Black lines illustrate the main zone of intertropical wind convergence (ITCZ), which is generally north of the rainfall maxima. Dashed black lines illustrate the Congo Air Boundary and red lines indicate the Equator and Tropics of Cancer and Capricorn. Reprinted from *Quaternary Science Reviews*, 124, Singarayer, J.S.. and Burrough, S.L., Interhemispheric dynamics of the African rain belt during the late Quaternary, 48–67. ©2015 with permission from Elsevier.

intervals, indicating reduced runoff and/or heavier isotopic values of the rainfall entering river systems, which might be expected with a reduction in monsoon (convective) rainfall. As there is no evidence that the ITCZ was displaced to the south of the east-west trending west African coastline (at ~5°N), together with the evidence already discussed, this suggests that the seasonal migration of the tropical rain belt was greatly reduced during Heinrich intervals. Today, maximum rainfall occurs ~5°–10° south of the zone of surface wind convergence (cf. Nicholson, 2018; Singarayer & Burrough, 2015; Figure 14). In fact, there is additional evidence that relatively dry conditions occurred during Heinrich intervals all across the equatorial zone of West Africa as far south as Angola (12°S). For example, Schefuβ et al. (2005) and Weijers et al. (2007) studied sediments in core GeoB 6518, recovered near the mouth of the Congo River, which drains a vast inland area (equal to 40% of the United States). δD of n-C_{29} alkanes (the main homolog of plant leaf waxes) was enriched during the Younger Dryas and THE1, indicating drier conditions prevailed within the vast Congo River catchment. With less freshwater entering the ocean, anomalously high $\delta^{18}O$ values in forams were also found. Branched glycerol dialkyl glycerol tetraethers (brGDGTs) derived from soils in the Congo Basin indicate that mean annual temperatures were 4°C –5°C cooler there during THE1 than in the late Holocene, while SSTs offshore were relatively warm (i.e., had cooled less). This increased the temperature gradient between the ocean and land surface would have favored offshore airflow, which (together with weaker South East Trade winds; Kim et al., 2003) may have led to a reduction in the flux of moist air from the ocean to the continental interior, resulting in less convective rainfall over the land area (Weijers et al., 2007).

In summary, offshore sediment records from the tropical and sub-tropical regions of west Africa provide a clear picture of reduced rainfall throughout the region during Heinrich intervals, with a strong increase in dust flux to the Atlantic within the Northeast Trade winds, as a result of a more limited seasonal migration of convective rainfall (the "African rain belt": Nicholson, 2018) associated with the ITCZ, and greater aridity across the Sahara/Sahel region. The southern (boreal winter) limit of the rain belt appears to have remained at around 5°N, but the northern (boreal summer) limit was more restricted. South of the ITCZ, a cooler land area and weaker trade winds led to less convective precipitation and lower rainfall totals. This picture is consistent with model simulations in which freshwater forcing is imposed in the North Atlantic to reduce the Atlantic Meridional Overturning Circulation (so-called hosing experiments). A reduction in AMOC leads to a southward shift in the summer (northernmost) position of the West African monsoon trough (ITCZ) by up to 4°–5° latitude and much drier conditions over the southern Sahara and Sahel with a strengthening of the African Easterly Jet stream and more dust advected offshore (Mulitza et al., 2008). Warming of the southern hemisphere (associated with a reduction in the AMOC) would also have led to the poleward migration of the Sub-Antarctic westerlies and a reduction in the strength of the Southeast Trade winds, contributing to less rainfall in those parts of Equatorial and sub-tropical Africa south of the ITCZ. The strong links between rainfall all across the northern part of the African continent can be seen in long records from the Gulf of Guinea and northwest Africa (Weldeab, 2012; Zarriess et al., 2011), recording Equatorial runoff and dust flux from the Sahara, respectively) as well as in an integrated record of runoff from the entire Nile river basin, seen in sediments from the SE Mediterranean off the Nile delta (Ehrmann et al., 2016). Similar millennial-scale variations are seen in all three records, indicating the strong control such variations exerted on the position of the African rain belt over the last glacial cycle (cf. Figures 13 and 15).

Continental proxy records of climatic conditions during Heinrich intervals are mainly provided by lake sediments, but records that extend back beyond THE1 are rare. Exceptionally dry conditions prevailed across

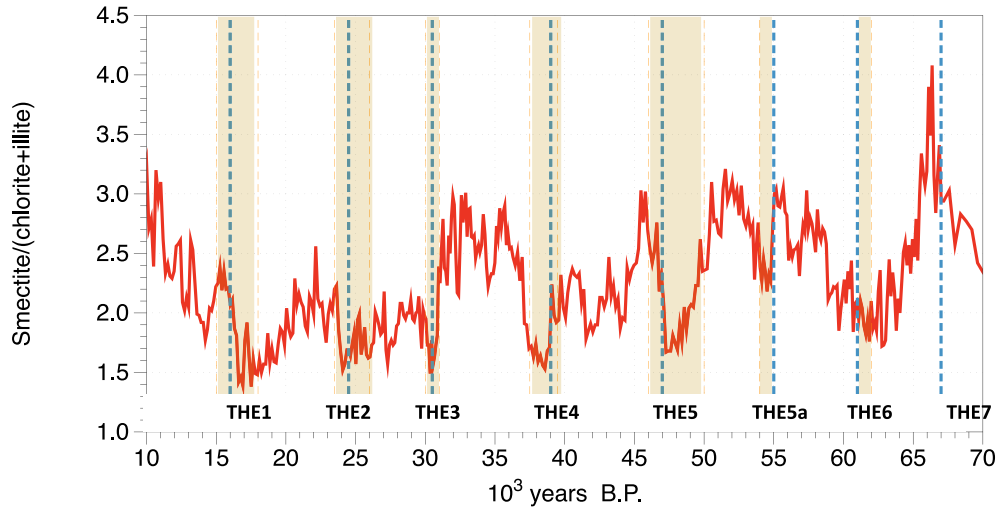

Figure 15. Smectite/(illite + chlorite) ratio, a proxy for discharge from the Nile and Atbara rivers, at site GeoTü SL110, northeast of the mouth of the River Nile in the eastern Mediterranean. Dashed blue lines indicate the timing of maximum IRD in the stacked record of 15 North Atlantic cores (normalized values, from Lisiecki & Stern, 2016). Shaded brown intervals indicate times when IRD exceeded median values for MIS2–4. Low smectite/(illite + chlorite) ratios indicate particularly arid conditions in the upper Nile watershed (modified, from Ehrmann et al., 2016). *Data source:* https://doi.org/10.1594/PANGAEA.71373.

much of sub-Saharan West Africa during the time of HE 1, with extreme drought occurring in some areas (Stager et al., 2011). In Lake Bosumtwi (6.5°N, in Ghana) submerged beaches at −60 m, dating to ~16.3 ka B.P., indicate much drier conditions (which led to more erosion of the exposed lake margins and higher sedimentation rates) during THE1. A similar pattern was seen during earlier HEs (HE2 to HE4; Shanahan et al., 2012). Magnetic susceptibility of the sediments also increased around the time of HE1 and HE2, most likely due to a higher concentration of iron sulfide minerals as a result of evaporative concentration of minerals caused by drought at those times (Peck et al., 2004). Exceptionally dry conditions were also recorded during HE 1 in sediments from a high elevation site in western Cameroon (Lake Bambili, ~6°N) (Lézine et al., 2013, 2019). Further south in Cameroon, sediment cores from Lake Barombi Mbo (~4.6°N) also show a sequence of dry episodes that (within radiocarbon uncertainties) appear to match closely the droughts seen at Bosumtwi. Estimates of precipitation changes during the last two HEs, based on pollen, suggest a 50% reduction in rainfall which resulted in a shift from the Guinea-Congolese forest biome that dominates the region today, to savanna, or an open savanna mixed forest (Lebamba et al., 2012).

Lakes Tana (12°N), Albert (~1.6°N), and Victoria (1°S) all became completely desiccated in THE1, resulting in the virtual cessation of Nile River outflow to the Mediterranean (Lamb et al., 2007; Marshall et al., 2011; Stager et al., 2002). Seismic reflectors in Lake Tana indicate that there were also earlier arid episodes (THEs) that may be related to Heinrich intervals HE2, HE4, and HE6 (Lamb et al., 2007). As moisture flux associated with the West African monsoon is restricted to the lower levels of the troposphere (Nicholson & Grist, 2003) and moist air from the Atlantic is limited by topography from penetrating far into tropical East Africa, the dominant moisture source for tropical East African rainfall is the Indian Ocean (Figure 14; Singarayer & Burrough, 2015). Thus, the pronounced reduction in rainfall (or P-E) seen in records throughout tropical East Africa must also have involved a significantly weaker flux of moisture entering the continent from the Indian Ocean (Berke et al., 2012; Tierney et al., 2008). In addition, a more restricted seasonal migration of convective rainfall toward the eastern margin of the West African monsoon further reduced rainfall north of the Equator (Figure 14).

South of the Equator, sediments from Lake Tanganyika (~7°S) provide strong evidence for recurrent dry periods associated with the Younger Dryas and Heinrich intervals HE1 and HE4, and possibly also HE5 and HE6 (Tierney et al., 2008). A similar situation is observed in Lake Challa (3°S) for HE1 and HE2, as recorded by δD in leaf waxes and lake level seismic reflection data (Moernaut et al., 2010; Tierney et al., 2011). In Lake Tanganyika, THE1 was exceptionally dry, more so than at any other time in the last 60,000 yr.

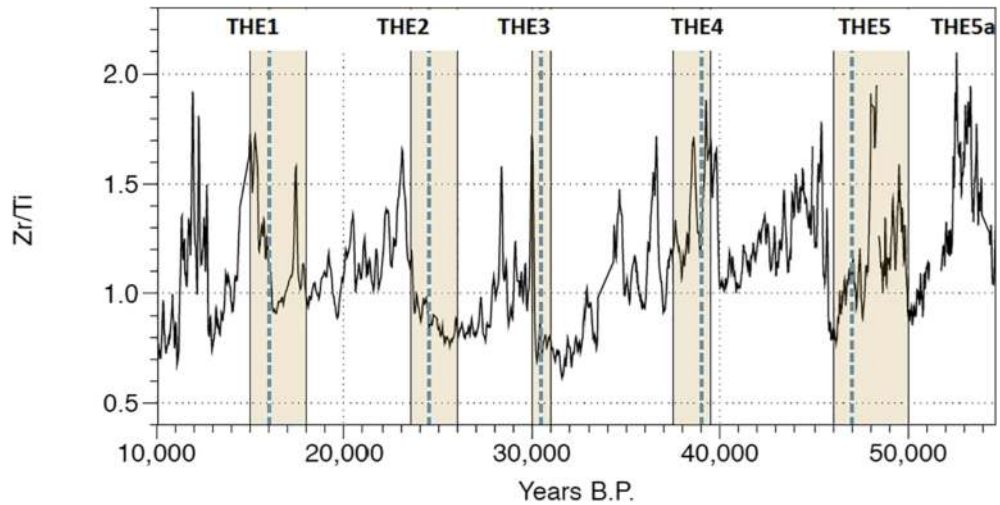

Figure 16. Zr/Ti ratio in Lake Malawi sediments. Peak values indicate high levels of aeolian sediment input from volcanic source rocks to the north of the lake, resulting from persistent NE winds as the ITCZ shifted to the south (Brown et al., 2007). Dashed blue lines indicate the timing of maximum IRD in the stacked record of 15 North Atlantic cores (normalized values, from Lisiecki & Stern, 2016). Shaded brown intervals indicate times when IRD exceeded median values for MIS2–4.

Although there is no obvious signal of Heinrich intervals HE2 and HE3, this is not the case further south in Lake Malawi (~10°S) where the elemental Zr/Ti ratio reflects the prevalence of northerly winds that deliver aeolian material from a large volcanic province to the north of the lake. Each of the Heinrich intervals (as well as the Younger Dryas period) is strongly recorded by peaks in Zr/Ti (Figure 16). Brown et al. (2007) interpret this as indicating the ITCZ (*sensu stricto*, which defines the southerly limit of winds from the north), must have been positioned south of the coring site for at least part of the year during each of the Heinrich intervals. This implies that there was a significant south/southwestern shift in the ITCZ and Congo air mass boundary, and associated rainfall during the boreal winter season (Thomas et al., 2012; cf. Figure 14). Such a scenario is supported by evidence of wetter conditions to the south of Lake Malawi, with Lake Chilwa (~15°S) more than doubling in the area at the times of H1, H2, and possibly H4 (Thomas et al., 2009) and increased runoff within the Zambezi River catchment, which had a higher flux of terrigenous material to the Indian Ocean during the YD and HE1 time periods (Just et al., 2014; Schefuβ et al., 2011; van der Lubbe et al., 2016;). There is also compelling evidence from the Middle Kalahari Desert (~21°S) that very large lakes developed in the Makgadikgadi Basin, coincident with several previous HEs (Burrough et al., 2009).

5. The Signal of THEs in Arabia and the Arabian Sea

There are very few continuous high-resolution paleoclimatic records from the Arabian Peninsula and the adjacent Persian Gulf, apart from a few stalagmite records that mainly cover wetter intervals when there was enough rainfall for groundwater flow in karst regions (Fleitmann & Matter, 2009). Two stalagmites from Moomi cave on Socotra Island in the Arabian Sea (~12°N), provide records that span the time intervals from ~11 to 27.5 ka and ~40–60 ka B.P., and so provide some insight into conditions during HEs 1, 2, and 5 (Burns et al., 2003, 2004; Shakun et al., 2007). The driest conditions recorded in Moomi cave (as indicated by the most enriched oxygen isotopes) occurred at around 47.7 ka B.P. Thereafter, calcite deposition became abruptly isotopically lighter, signifying a rapid shift to wetter conditions, within a period of ~25 yr (Burns et al., 2003). Other periods of isotopic enrichment occurred at ~16.4 ka and 23 ka B.P., around the times of HEs 1 and 2 in the North Atlantic (Shakun et al., 2007). As Socotra rainfall is mainly related to the seasonal migration of the ITCZ across the island (as well as from tropical cyclones during boreal summer) periods of extreme aridity are due to convective rainfall associated with the ITCZ staying south of the island, and less cyclonic rainfall.

Another source of information about terrestrial conditions in the Arabian Peninsula and adjacent Persian Gulf is provided by sediment cores from off the Indus fan in the northern Arabian Sea, which provide a

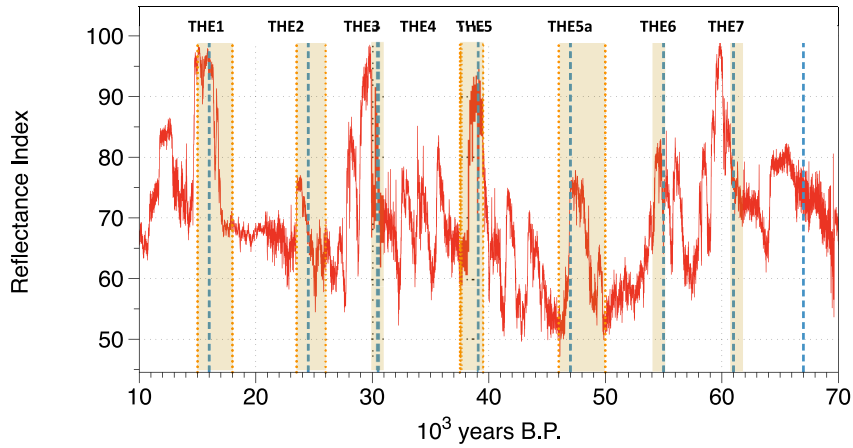

Figure 17. Color Reflectance index ("L1") in sediments from marine sediment core SO130-289 KL (23.1°N, 66.5°E, in the northeastern Arabian Sea). Lower values are darker, organic-rich; higher values correspond to periods with high levels of terrigenous sediment input (data from Deplazes et al., 2013). Dashed blue lines indicate the timing of maximum IRD in the stacked record of 15 North Atlantic cores (normalized values, from Lisiecki & Stern, 2016). Shaded brown intervals indicate times when IRD exceeded median values for MIS2–4. *Data source:* https://doi.org/10.1594/PANGAEA.815882.

remarkable history of aeolian activity on land areas to the west. Under modern conditions, strong southwesterly monsoon winds cause upwelling and high nutrient levels which lead to high marine productivity and depletion of oxygen as organic matter is remineralized. Consequently, sediments are dark and organic-rich, but when the monsoon was weaker and upwind regions were drier, there was an increase in aeolian input and a reduction in organic productivity, resulting in lighter-colored sediments. Furthermore, wind-blown terrigenous material from Arabia has a distinct geochemical signature (relatively high in Mg/Al and Ti/Al) and has a higher median grain size compared to sediments from the Indus river. Thus, variations in sediment color (total reflectance, L*), geochemistry and grain size all enable changes in aridity and dust transport to the adjacent ocean to be tracked through time, with the lightest colored sediments (high L*) signifying periods of abundant aeolian deposition (Figure 17; Deplazes et al., 2013, 2014). In this way, THEs are clearly recorded as intervals when high levels of aeolian dust were transported to the site, signifying a weak Indian summer monsoon and extremely arid conditions upwind over Arabia and the Persian Gulf. Each of these events began and ended relatively abruptly.

6. The Signal of THEs in India

Rainfall across India is primarily related to the summer monsoon, which progresses northward across the continent from June onwards, continuing into September in most years. Rainfall is depleted in ^{18}O during the transport of moisture into the continental interior, resulting in isotopically light calcite deposited in speleothems during periods when monsoons are strongest (i.e., producing more intense rainfall, and/or prolonged periods of rain). In contrast, weaker monsoons are isotopically enriched (Kaushal et al., 2018). There are few records within India that span HEs, but a long record from northern India (Bittoo cave) extends from ~12 to 70 ka B.P. providing a long-term perspective on monsoon rainfall during HE1-HE6 events at the northern limit of the monsoon system in the sub-continent (Kathayat et al., 2016). Although overall variations in $\delta^{18}O$ were driven by orbital forcing on the precessional timescale, superimposed on those long-term fluctuations were abrupt shifts in isotopic values during each HE, signifying particularly low monsoon rainfall, with the most isotopically enriched period during THE1 (Figure 18). A similar record was found at the time of HEs HE1 and HE2 in Mawmluh cave, northeastern India (Dutt et al., 2015). Today, both caves receive monsoon rainfall from the Bay of Bengal with drier periods occurring when airflow from that region is weak. Back trajectory analysis of air masses reaching Bittoo cave indicate that drier years are associated with isotopically enriched rainfall coming from local sources and the Arabian Sea, as well as increased airflow from the Westerlies, which tends to limit convective rainfall (Kathayat et al., 2016, Supplemental).

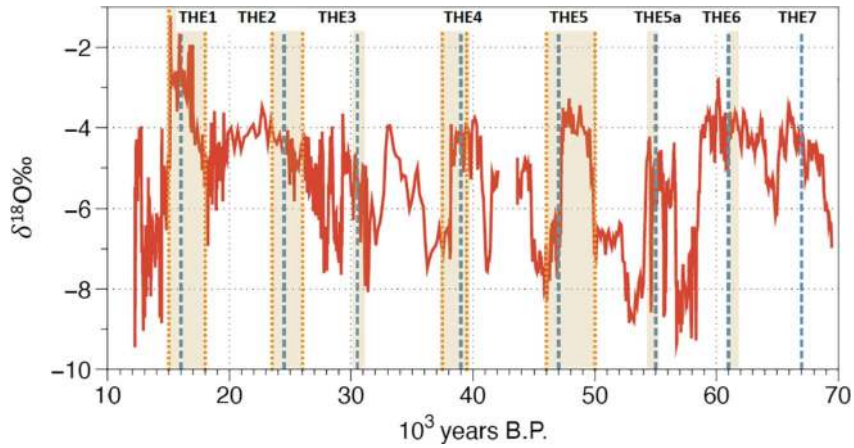

Figure 18. Oxygen isotope record for the last 70 ka from Bittoo cave, northern India. Less negative values signify monsoon failures (data from Kathayat et al., 2016). Dashed blue lines indicate the timing of maximum IRD in the stacked record of 15 North Atlantic cores (normalized values, from Lisiecki & Stern, 2016). Shaded brown intervals indicate times when IRD exceeded median values for MIS2–4. *Data source:* https://www.nature.com/articles/srep24374#Sec7.

There are very few other terrestrial records from India that provide paleoclimatic data spanning HEs, but sediment cores from the Bay of Bengal, offshore of the Godavari and Mahanadi rivers that drain much of central India (Figure 2), provide an integrated view of conditions on the continent. Pollen analysis clearly shows that during the time of HE2, 70% of pollen came from grassland vegetation, with only 10% from biomes associated with a wetter climate, indicating that relatively dry conditions prevailed across most of the interior of India at that time (Zorzi et al., 2015). Similarly, oxygen isotopes in planktonic forams from sediment cores taken off the eastern coast of India in the Bay of Bengal indicate a period of higher salinity (enriched $\delta^{18}O_{sw}$) during THE1. Today monsoon rains and major river discharge create a strong freshwater salinity gradient across the Bay of Bengal, but this was evidently weakened during THE1 due to a reduction in monsoon rainfall over India (Govil & Naidu, 2011; Rashid et al., 2011).

In the absence of a more extensive network of terrestrial records, it is difficult to map out the geographical pattern of monsoon reduction across the interior of the sub-continent. Nevertheless, the evidence available indicates that the most recent North Atlantic HEs were also associated with exceptional THEs across India as a result of weaker monsoon rainfall, a picture that is also seen across parts of Southeast Asia, as discussed in the next section.

7. The Signal of THEs in China, Southeast Asia and Northern Australia

The seasonal migration of the ITCZ is greatest over SE Asia and southern China, producing a strong seasonal cycle of convective monsoon rainfall (Figure 5). Over southern China, air masses associated with the Indian monsoon bring moisture from the south and southwest. Moist air from the Pacific also enters the region from the east and southeast, later in the summer months (the East Asian monsoon) as the locus of maximum rainfall shifts northward (H. Zhang et al., 2018; Zhao et al., 2010). However, by far the main source of moisture for monsoon rainfall over most of southern and central China is the Indian monsoon (Baker et al., 2015; Maher & Thompson, 2012; Yang et al., 2016). The penetration of monsoon rainfall inland is strongly linked to the position of the Westerly jet stream which is south of the Tibetan plateau in winter months, but shifts northward in May–June, bringing the "Meiyu" rainfall to central China. Chiang et al. (2015) argue that a cool Asian continent resulting from a reduction in the AMOC during HEs could have restricted the jet from transitioning to north of the plateau, limiting rainfall across a wide area of China.

Over the last decade, a plethora of well-dated stalagmites from caves in southern and central China) have provided high-resolution $\delta^{18}O$ records (all between 24° and 32.5°N: Table 2) that span (at least) the last 70 ka, providing a broad view of changes in the summer monsoon (Table 2, Figure 19). In all cases, the

Table 2
Chinese Cave Stalagmites That Record Major Tropical Hydroclimatic Events

Name	Latitude (N)	Main reference
Hulu	32.50	Y. Wang et al. (2001)
Sanbao	31.67	Zhao et al. (2010)
Yongxing	31.58	Chen et al. (2016)
Qingtian	31.20	W. Zhang et al. (2014)
Xinya	30.75	T. Li et al. (2007)
Haozhu	30.41	H. Zhang et al. (2018)
Yangzi	29.78	Wu et al. (2020)
Furong	29.13	T. Li et al. (2011)
Yangkou	29.03	T. Zhang et al. (2017)
Sanxing	27.37	Jiang et al. (2014)
Daishibao	26.08	Zhao et al. (2010)
Wulu	26.05	Duan et al. (2014), Liu et al. (2010), and Zhao et al. (2010)
Dongge	25.28	Yuan et al. (2004)
Xiaobailong	24.12	Cai et al. (2006, 2015)

long-term records (which track precessional forcing) are punctuated by abrupt episodes of isotopic enrichment that define each of the Chinese THEs as times when the summer monsoon was weak. But the term "weak monsoon" is rather imprecise; $\delta^{18}O$ of rainfall is mainly a function of the vapor lost through condensation between the oceanic source and the location of rainfall (i.e., integrated moisture transport; Cheng et al., 2012, 2019; Hu et al., 2019; Maher & Thompson, 2012). A "strong" monsoon implies strong advection of moisture into the interior of China, presumably leading to high amounts of convective rainfall, with depletion of heavy isotopes. A "weak" monsoon suggests less isotopic depletion due to a reduction in upstream "rainout," lower amounts of moisture advected, and lower rainfall amounts (Pausata et al., 2011). But *quantifying* the relationship between isotopic enrichment and actual rainfall amount is not straightforward. Indeed, H. Zhang et al. (2018) used trace elements as an independent measure of rainfall amount and found little change during the most isotopically enriched interval seen in $\delta^{18}O$ during THE1. Furthermore, Clemens et al. (2018) found no clear signal of precession-related enhanced runoff in sediment cores from off the mouth of the Yangtse River during times when isotopically depleted intervals are seen in stalagmites

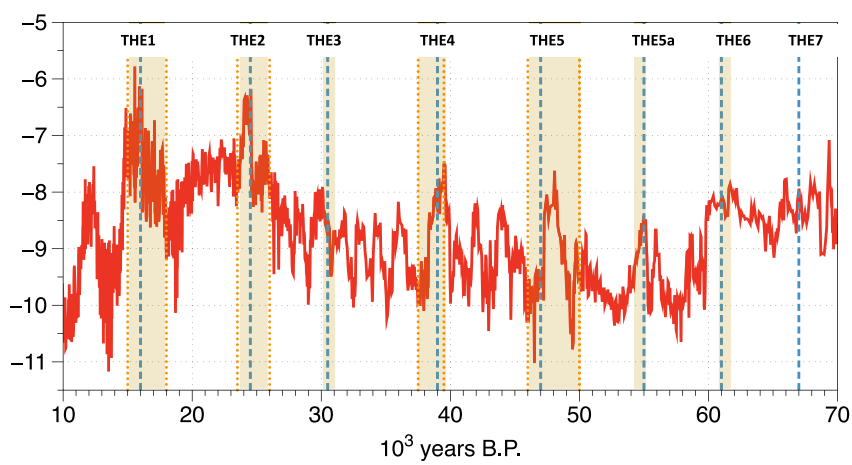

Figure 19. Composite $\delta^{18}O$ record from Sanbao cave, central China (from Cheng et al., 2016). Weak monsoon episodes are indicated (THEs 1–7). Dashed blue lines indicate the timing of maximum IRD in the stacked record of 15 North Atlantic cores (normalized values, from Lisiecki & Stern, 2016). Shaded brown intervals indicate times when IRD exceeded median values for MIS2–4. *Data source:* https://www.nature.com/articles/nature18591#Sec15.

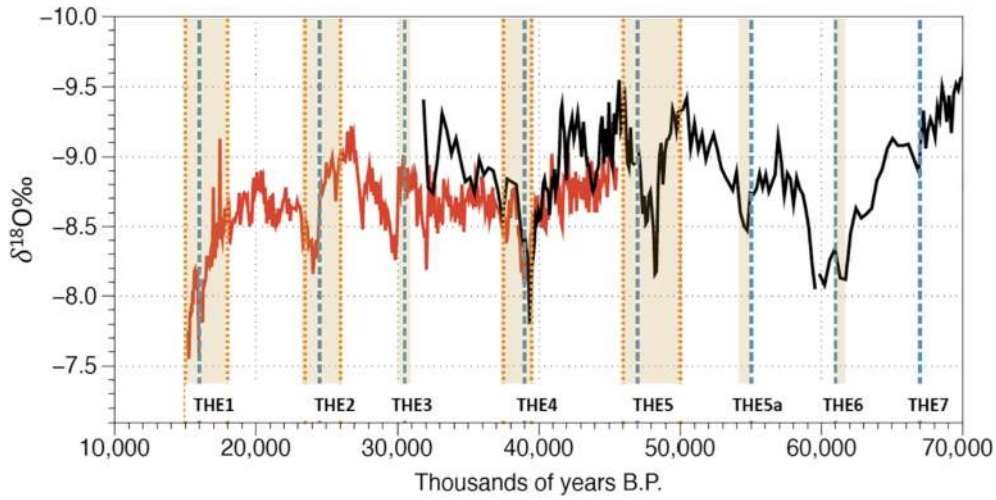

Figure 20. Two stalagmite $\delta^{18}O$ records from caves in Gunung Mulu National Park, Northern Borneo, Malaysia (4.1°N, 114.83°E): Bukit Assam Cave stalagmite BA02 (red) and Secret Cave stalagmite SC02 (black). Weak monsoon episodes (higher $d^{18}O$ values) are indicated (THEs 1–7). Dashed blue lines indicate the timing of maximum IRD in the stacked record of 15 North Atlantic cores (normalized values, from Lisiecki & Stern, 2016). Shaded brown intervals indicate times when IRD exceeded median values for MIS2–4. (data from Carolin et al., 2013). *Data source:* https://www.ncdc.noaa.gov/paleo-search/study/14515.

from the Yangtse valley. However, in Huguang Maar, a lake in southeast China (~21°N), high levels of titanium (from aeolian sediments) are inversely correlated with Hulu cave $\delta^{18}O$, suggesting that a southward shift of the ITCZ led to both reduced summer rainfall and a strong winter monsoon with increased aeolian influx (Yancheva et al., 2007). A similar conclusion was reached by Han et al. (2015), who found increased aeolian sand activity around the time of HEs. Although the actual magnitude of rainfall reduction during isotopically enriched (THE) intervals is unclear, there is no doubt that there were abrupt and significant disruptions of monsoon airflow around the time of North Atlantic HEs across much of southern and central China.

There are only a few sites within the tropics (*sensu stricto*) of Southeast Asia that span the time of North Atlantic HEs (H. Zhang et al., 2019). Nevertheless, those records show significant THEs, resulting from a reduction in monsoon airflow (either via India and the Bay of Bengal or from the western Pacific) and associated rainfall. A stalagmite from Thuong Thien Cave near Hanoi in northern Vietnam shows that rainfall was isotopically enriched during two intervals that partly overlap with HEs HE2 and HE3 (Dung et al., 2020). This signal is similar to the record from caves in northern Borneo (~4°N) in which strong isotopic enrichment occurred during HE1-HE6 with additional abrupt THEs at ~55 ka and 73.42 ka B.P. (the latter possibly linked to the mega-eruption of Toba, dated at 73.88 ka B.P.; Carolin et al., 2013; Partin et al., 2007; Figure 20). Evidence from sediment cores south of Sumatra (0.5°–3°N) also indicates higher salinity levels (an indicator of reduced local rainfall and terrestrial runoff) during HEs HE1 to HE4 (Mohtadi et al., 2014).

Another stalagmite from south of the Equator, from the island of Flores in Indonesia (8°S) provides a complementary proxy of monsoon rainfall spanning HE1 (Ayliffe et al., 2013). In this record, isotopic depletion records an increase in monsoon intensity (i.e., a higher percentage of annual rainfall from summer convective rainfall) just as proxies from north of the Equator record anti-phased isotopic enrichment. This indicates that there was a latitudinal shift in the ITCZ that moved the locus of maximum summer rainfall to the south. High levels of ^{232}Th, an indicator of terrestrial weathering and river erosion, deposited offshore north of Flores at the time of HE1 (Muller et al., 2012) and in another core from south of Papua New Guinea (for HE2 and HE4; Shiau et al., 2011) also indicate an increase in rainfall across the region. Further south (~17°S) stalagmites from Ball Gown Cave in Western Australia and peat deposits in Lynch's Crater in northeastern Australia provide additional evidence for stronger Australasian monsoon rainfall during HE1 and HE2 (Denniston et al., 2013; Muller et al., 2008).

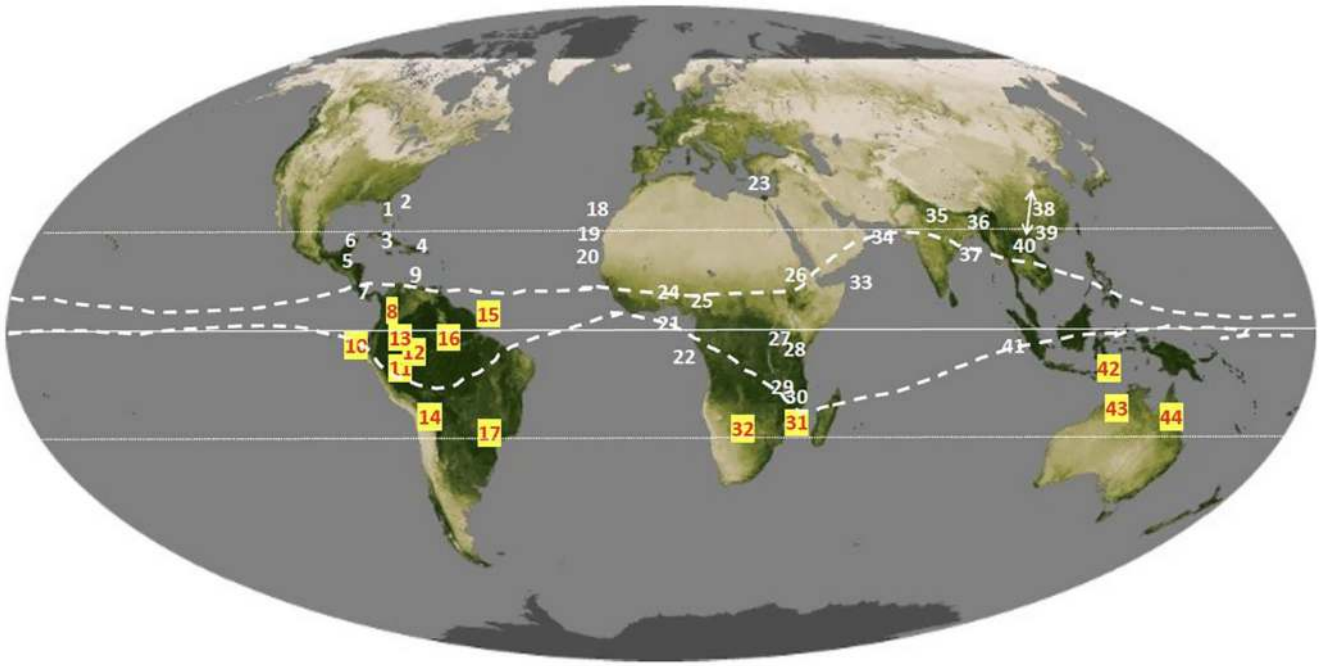

Figure 21. A summary figure showing the areas where increased rainfall was recorded during THEs (locations in yellow) and areas where rainfall was reduced (locations in white; cf. Figure 2). The modern seasonal range of the ITCZ is shown by the dashed lines. Note that not all THEs are represented by proxies at the locations shown, and individual THEs may have varied in amplitude and duration, as discussed in the text, and so this figure should be viewed with those caveats in mind.

All of the evidence from Southeast Asia, together with the records from northern India and southern and Central China, points to repeated reductions in monsoon strength across a vast region of south and Southeast Asia (and a strengthening of the monsoon regime further south) around the time of North Atlantic HEs. The key feature of all these events is the abruptness of the onset and termination of each THE, and their regional synchrony. Thanks to high-precision uranium-series dating, it is clear that in some cases the switch from strong to weak monsoon (and back again) occurred over the course of just a few decades (e.g., W. Zhang et al., 2014). Given this widespread and more or less synchronous change that characterizes THEs all across the vast region of monsoon Asia, the first order explanation points to a widespread weakening and/or major geographical shift of the entire summer monsoon system that would otherwise deliver heavy rainfall right across the region (north of the Equator). Furthermore, the rapidity with which isotopic changes took place (at both the start and end of THEs)—in a matter of decades—suggests that the changes were a direct atmospheric response to forcing, originating in the North Atlantic rather than from relatively slower changes via the oceanic circulation.

8. Discussion

THEs, characterized by extreme regional rainfall anomalies, were a recurrent feature of marine isotope stages 2–4 and involved some of the most abrupt and dramatic changes in the late Quaternary climate system. Some areas became exceptionally dry, while at the same time, other regions became unusually wet (Figure 21). Such changes often occurred within a few decades and must have had significant consequences for many ecosystems, forcing the migration of some species in order to stay within a suitable habitat, and isolation or perhaps even the local extinction of others that were unable to adapt to the rapidity of the changes (cf. Kaufman et al., 1997; Seehausen, 2002).

It has long been accepted that a large increase of freshwater in areas of the North Atlantic where convective overturning occurs, would increase the stability of the water column and reduce the AMOC, an idea first expounded by Broecker et al. (1985). Where the freshwater might have come from (and why) remains uncertain, and we offer no commentary on that. But the connection between ice-rafted debris (HEs),

freshwater forcing and AMOC stability is critically important for our discussion of changes in tropical circulation, particularly the trajectory and ultimate distribution of freshwater in the North Atlantic (cf. Roche et al., 2010). In this review, we have often associated THEs with HEs, but the challenges of precisely dating marine sediments make it difficult to determine the exact sequence of events, which may have transpired over a century or less. For example, Hodell et al. (2017) in a detailed study of HE1 in a sediment core from the central North Atlantic found 2 distinct peaks in IRD (at Site U1308, 49.88°N; 24.23°W); the central [calendar year] dates on these are 16.2 and 15.1 ka B.P. (with 2 sigma ranges of 15.5–17.1 and 14.3–15.9 ka B.P., respectively). However, more precise dating is constrained by issues of bioturbation (particularly at the end of IRD events) and uncertain corrections for the oceanic radiocarbon reservoir (which may have changed considerably during these IRD events). Inconsistent radiocarbon ages given by different species of forams selected from the same core depth, and changing atmospheric radiocarbon concentrations over the time of interest can also pose problems (Hodell et al., 2017). Furthermore, most records of IRD are expressed as % IRD, which leaves the variations subject to changes in the content of other sediments (e.g., dissolution of foraminifera). IRD fluxes (deposition rate per unit area per unit time) reconstructed from the ^{230}Th-normalized burial flux of IRD provide an alternative record, but such estimates are rare (Zhou et al., 2021). Finally, the timing and magnitude of IRD deposition in other locations might have been somewhat different than that registered at the mid-Atlantic site examined in detail by Hodell et al. (2017). For example, Condron and Hill (2021) showed that icebergs scoured sediments off the eastern coast of the U.S. as far south as southern Florida during HE3, indicating that a coastal current of freshwater may have been particularly effective at carrying icebergs away from the North Atlantic Ruddiman Belt at that time. This may explain why the IRD stack (and ^{231}Pa/^{230}Th discussed below) show a smaller signal at the time of HE3 compared to other events. If the movement of icebergs and associated freshwater was fundamentally different during HE3, it may explain why many paleoclimatic records from across the tropics did not register a strong perturbation at that time. Despite all of these issues, a "stacked" set of 15 IRD records from the North Atlantic shown in Figure 1 nevertheless shows remarkable temporal synchrony with proxies of THEs (though see the caveats in caption to Figure 1; Lisiecki & Stern, 2016). Within the uncertainties of dating, tropical rainfall anomalies occurred very close in time ($\pm 10^2$–10^3 yr) to the deposition of North Atlantic IRD, a conclusion which concurs with that of Jullien et al. (2007) and Liang et al. (2020) and is analogous to the conclusions of Corrick et al. (2020) who compared the timing of DO events in Greenland ice with independently dated tropical stalagmite records.

To examine these connections further, Figure 22 compares the stacked IRD record of Lisiecki and Stern (2016) with a proxy of AMOC strength, ^{231}Pa/^{230}Th, in sediments from the western North Atlantic (Böhm, 2014; Lippold et al., 2009; McManus et al., 2004). Again, within the limits of dating, IRD and AMOC strength are closely linked, both in time and amplitude. This, in turn suggests that even though there may have been considerable amounts of freshwater entering the North Atlantic—without any associated sediment—prior to the release of sediment-loaded icebergs from calving glaciers (cf. Bradley & England, 2008) the IRD record is in fact a good proxy for the amount and distribution of the *additional* freshwater forcing that was necessary to bring about a drastic reduction in AMOC strength during each HE; the freshwater associated with IRD pushed the AMOC "over the edge." As a consequence of a reduction or cessation of the AMOC, cooling of the North Atlantic and adjacent continents took place, though model simulations (and simple energy flux considerations) suggest that this alone was insufficient to account for the observed temperature changes around the margins of the North Atlantic (Seager & Battisti, 2007). Several studies argue that the magnitude of cooling must also have involved a sudden expansion of sea-ice, especially in winter (Chiang & Bitz, 2005; C. Li et al., 2005). This then led to a rapid atmospheric response involving the southward displacement of the ITCZ, and associated anomalous hydroclimatic events (both wet and dry) throughout the tropics (THEs) and (as a result of the AMOC slowdown) the accumulation of heat in the southern hemisphere oceans (Chiang & Friedman, 2012).

High resolution ice core records of CH_4 and CO_2 (and associated isotopic data) show abrupt increases in these gases over the course of HE1, 4, and 5, which may have resulted from wetland expansion over land areas in the southern hemisphere where rainfall greatly increased (Bauska et al., 2021; Rhodes et al., 2015). These data provide important additional constraints on the timing and duration of THEs in the tropics. It is also of interest that several paleoclimatic records show evidence of sub-stages within THEs (e.g., in THE1: Bouimetarhan et al., 2012; Dupont et al., 2010; Hodell, Anselmetti, et al., 2008; Huang et al., 2019; Stríkis

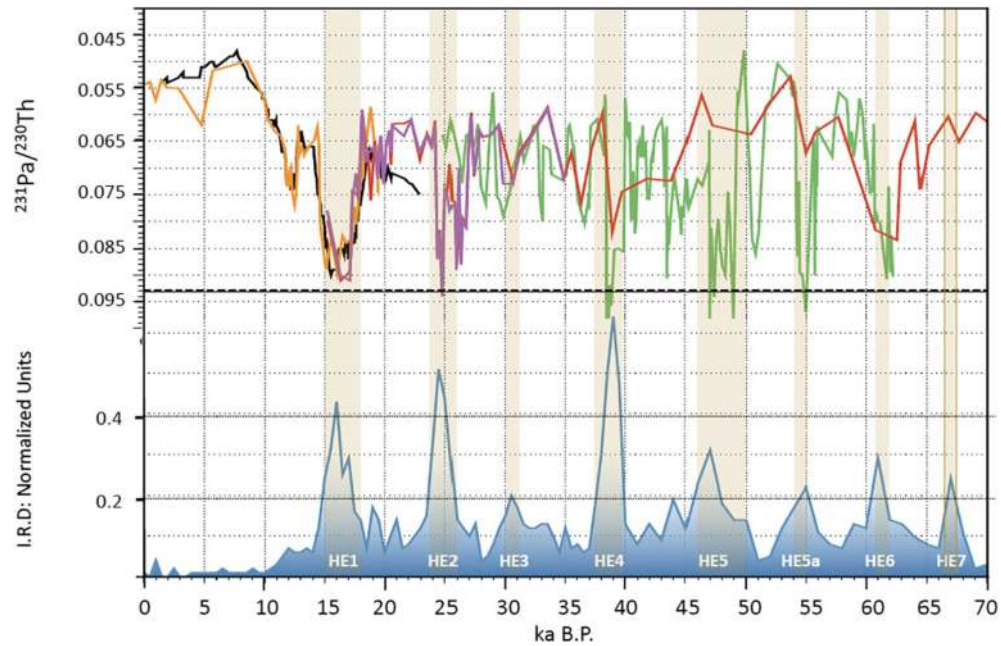

Figure 22. ^{231}Pa/^{230}Th in several North Atlantic sediment cores; values of >0.093 (dashed black line) represent a complete cessation of North Atlantic deepwater formation (note data are plotted inversely; from McManus et al., 2004, in orange; Lippold et al., 2009, in purple; Böhm, 2014, in red; Henry et al., 2016, in green; Ng et al., 2018, in black, 9-point running mean). Lower blue line is the stacked record of IRD based on 15 North Atlantic cores (normalized values, from Lisiecki & Stern, 2016). Shaded brown intervals indicate times when IRD exceeded median values for MIS2–4. Data sources: https://www.ncdc.noaa.gov/paleo-search/study/6406; https://www.ncdc.noaa.gov/paleo-search/study/20248.

et al., 2015 and in THE4 and 5: Kanner et al., 2012). These are reminiscent of Hodell et al.'s (2017) North Atlantic sediment record, which also suggests that there were two pulses of sediment deposition, as noted earlier, as well as ice core evidence for multiple stages within Heinrich stadial 4 (Guillevic et al., 2014). As more high-resolution, well-dated terrestrial records become available, it may be possible to decipher in more detail the precise sequence of changes that took place within the North Atlantic and across the tropics.

It is important to recognize that abrupt hydroclimatic changes in the tropics and sub-tropics (THEs) were superimposed on low-frequency climate fluctuations resulting from precessional forcing, which strongly modulates rainfall in those regions on timescales of 10^4–10^5 yr. This may have led to a somewhat different response to freshwater forcing over MIS2–4, depending on the phase of the precessional cycle at the time. In addition, the growth of continental ice sheets affected the global atmospheric circulation, and in some areas, particularly Southeast Asia, the extent of continental land area exposed due to sea-level changed significantly, affecting both ocean circulation and regional atmospheric dynamics. The effect of freshwater disruptions to the AMOC thus played out on a moving target, in both time and space. Although transient model simulations that span multiple precessional cycles do not yet exist, simulations for selected time intervals have been made and they provide insight into how the atmospheric circulation responded to these different factors (e.g., Singarayer et al., 2017). Changes in precession lead to an overall latitudinal expansion or contraction of the tropical rainfall belt (particularly over oceanic regions), whereas the presence of large continental ice sheets, and freshwater forcing in the North Atlantic resulted in a southward shift in the axis of tropical rainfall in both boreal summer and winter months (Singarayer et al., 2017).

Numerous Global Climate Model simulations have examined the tropical response to imposed freshwater forcing in the North Atlantic, compared to either modern or LGM conditions (e.g., Atwood et al., 2020; Cheng et al., 2007; Chiang et al., 2008; Kageyama et al., 2013; Seager & Battisti, 2007; Stouffer et al., 2006; Vellinga & Wood, 2002; R. Zhang & Delworth, 2005). Although it has been pointed out that most of these studies place freshwater in a location of the North Atlantic (50°–70°N) which was probably not affected by drainage from the Laurentide Ice Sheet (Condron & Winsor, 2011, 2012) and also that they commonly

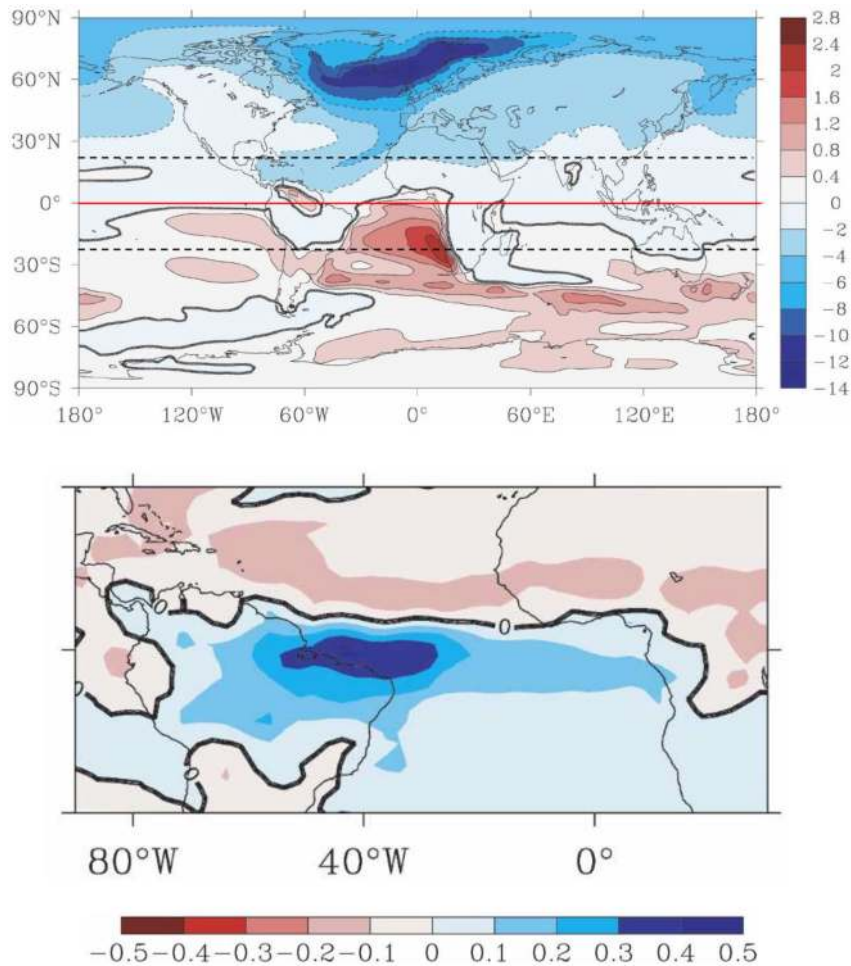

Figure 23. (Above) Ensemble mean surface air temperature anomalies (°C) and (below) precipitation anomalies (mm d^{-1}) (both relative to the reference period mean) during years 81–100 after 1sv of freshwater was imposed on the North Atlantic from 50° to 70°N (based on 9 AOGCMs) (Stouffer et al., 2006). © American Meteorological Society. Used with permission.

impose volumes of freshwater that are unrealistic in magnitude (Bradley & England, 2008), they nevertheless provide some insight into the consequences and temporal evolution of a slowdown or complete shutdown of the AMOC, regardless of the actual cause. Whether such changes were originally initiated elsewhere (e.g., in the Tropical or North Pacific; Clement et al., 2001; Seager & Battisti, 2007; Walczak et al., 2020) is an open question and one which we do not address here.

All simulations involving freshwater forcing produce cooling across the northern hemisphere (decreasing away from the North Atlantic), a southward shift in the ITCZ and associated rainfall, and a slight increase in mean air temperature over the southern hemisphere (Figure 23), but the regional details vary depending on the model used and the magnitude of the imposed forcing. Lower temperatures lead to high-pressure anomalies over continental areas, which reduce monsoon airflow from the tropical oceans (Dong & Sutton, 2002). In addition, there is less convective activity over the cooler northern continental tropics and so rainfall amounts are correspondingly reduced (Singarayer et al., 2017). Several authors have noted that ocean heat transport into the North Atlantic (~0.4 PW today) is far less than that transported by the atmosphere (Seager et al., 2002; Trenberth & Caron, 2001), and any reduction in that flux would be compensated for by an increase in the cross-equatorial atmospheric heat flux. However, the cooling recorded by mid-latitude paleoclimate proxies on land is far greater than would be expected from a reduction in AMOC alone (Cheng et al., 2007; Seager & Battisti, 2007). This suggests that an additional factor, a massive expansion of winter sea-ice cover in the North Atlantic due to a reduction in the ocean heat flux, must have been associ-

ated with a slowdown in AMOC (and in fact probably contributed to a further reduction in AMOC due to feedback effects; W. Cheng et al., 2007; Chiang & Bitz, 2005; C. Li et al., 2005). An expansion of sea ice extent would have increased the surface albedo and drastically reduced net radiation across the North Atlantic, leading to much lower temperatures (advected southward by the sub-tropical ocean gyre circulation) and further increasing the interhemispheric temperature gradient (Cheng et al., 2007). This would then have led to a rapid atmospheric response—within less than a decade from the onset of freshwater forcing—in which the ITCZ and Hadley circulation shifted southward (cf. Figure 3), increasing atmospheric heat transport into the northern hemisphere in order to balance the hemispheric asymmetry in temperature (Broccoli et al., 2006; Donohoe et al., 2013; McGee et al., 2014). In effect, the atmospheric response acted as a "bridge" that quickly transferred the oceanic changes within the Atlantic Basin to other areas of the globe (Dong & Sutton, 2002).

A robust conclusion of model simulations is the strong relationship between changes in atmospheric heat transport and the mean latitude of maximum precipitation in the equatorial zone: a ~0.3 PW increase in northward atmospheric heat flux corresponds to a 1° southward shift in the mean location of the ITCZ, a quantity that is similar on both seasonal and longer timescales (Donohoe et al., 2013; McGee et al., 2014). As the convergence zone shifted southward, a wind-evaporation-SST feedback in the Atlantic also likely developed as stronger Trade winds increased evaporation over the ocean, lowering SSTs and extending the anomalous cooling further south, further increasing the SST gradient in the sub-tropical Atlantic (Chiang et al., 2008; Chiang & Friedman, 2012). Whether the amount of convective rainfall was reduced within convective plumes as a result of cooler SSTs, due to a reduction in convective available potential energy is an open question (Evans & Webster, 2014; Folkins & Braun, 2003; Graham & Barnett, 1987). However, model simulations by Singarayer et al. (2017) indicate that local thermodynamic effects strongly influenced rainfall amounts over continental regions, due to cooler conditions and lower humidity levels. With a reduction or shutdown of the AMOC, heat would have accumulated at depth in the North Atlantic due to the suppression of ocean convection, allowing the AMOC to become re-established fairly quickly later on, when convective overturning eventually resumed (Knutti et al., 2004). Based on TRACE21 transient model simulations, McGee et al. (2014) point out that one additional consequence of these changes was a reduction in the amount of time that the ITCZ would have been positioned in the northern hemisphere (by ~ 1 month per year during HE1) with the seasonal migration into the southern hemisphere occurring ~1 month earlier in the (boreal) Fall. Thus, the rainy season was prolonged in those areas of the southern hemisphere toward which the convective rain belt was displaced.

An interesting result of the transient climate evolution of the last 21,000 yr (TRACE21) model simulation of HE1 is that the *overall* shift in ITCZ position was quite small, <1° of latitude. McGee et al. (2014) estimated that the inter-hemispheric temperature gradient increased by 0.29 ± 0.22 K compared to today, which led to a southward shift in the ITCZ (defined by the centroid of near-equatorial precipitation) of 0.61° ± 0.47°, and an increase in atmospheric heat transport of 0.22 ± 0.18 PW (all values are for the global mean response). A similar result was found by Roberts et al. (2017). This reflects the fact that over the oceans, there was little change in the location of the convergence zone. However, while such studies provide insight into the overall energetics of the tropical climate system and how it might be expected to respond to a sudden cooling of the North Atlantic Basin, hydroclimatic changes on the tropical continents reflect regional dynamics that are superimposed on these large-scale circulation changes. In the Americas, cooler sub-tropical SSTs and a southward shift in the ITCZ led to a dramatic reduction in rainfall over Central America, as even seasonal changes in the Hadley circulation did not result in significant convective activity across the region (cf. Figures 5 and 23). Further south, over northern South America, a longer rainy season, and enhanced moisture flux into the continental interior increased total rainfall amounts and extended the austral summer rains as far as 27°S. Isotopic records found in speleothems throughout the region record the increase in convective rainfall, and distinctive geochemical signatures in offshore sediments indicate enhanced runoff from the Amazon Basin (Figures 9–12). The hydroclimatic consequences of all these changes are well-documented in a diverse set of paleoclimate records extending from Bolivia and southern Brazil to Guatemala and the northern Caribbean.

In West Africa, the main locus of tropical rain shifted into the southern hemisphere, and higher pressure (increased subsidence) and stronger northeasterly winds suppressed rainfall further north. As a result, aridity

was enhanced across the southern Sahara, the Sahel-Saharan ecotone shifted southward by ~4° (~450 km), and active dunefields developed as far as 14°N in Senegal. Unlike South America, rainfall in the equatorial zone did not increase; there is strong evidence that the entire Congo Basin was drier, at least during North Atlantic HE1, and similar conditions prevailed across the continent to the east, with a drastic reduction in Nile River outflow. Relatively dry conditions may also have extended as far as 12°S, into Angola and to the east as far south as Lake Malawi (10°S). However, further south and east, hydroclimatic conditions were much wetter, with higher rainfall amounts over the Zambezi drainage and extensive lakes developing at 21°S in the modern day Kalahari Desert. Weaker southeast Trade winds, a more limited seasonal migration of the tropical rainfall belt and significantly less moisture advected into East Africa from the Indian Ocean all contributed to the remarkable hydroclimatic changes observed across the entire region (Figures 13–16).

Across monsoon Asia—from the Arabian Peninsula to China—abrupt THEs are recorded in a large number of paleoclimate archives. Throughout the region, relatively dry conditions prevailed during HEs as the flux of moisture from the oceans to the continents was reduced, rainfall was more isotopically enriched, and in some areas, the atmospheric dust load increased (Figures 17–20). These changes were primarily the result of a southward shift in the seasonal migration of ITCZ over the Indian Ocean and adjacent areas of Southeast Asia, perhaps exacerbated by cooler SSTs across the region. To the north, cooler conditions over the Eurasian continent resulted in higher pressure over the land area, which reduced monsoon airflow (from both the Indian and the East Asian monsoon systems). The usual seasonal migration of the westerly jet (from south of the Tibetan Plateau to the north) may also have been suppressed, resulting in limited penetration of moisture-bearing winds from the Bay of Bengal into southern China. Similarly, dry THEs were also recorded across Southeast Asia north of the Equator, from Sumatra to Vietnam, while wetter conditions prevailed south of the Equator, where isotopically light rainfall is recorded in speleothems from the island of Flores, and in northern Australia.

In summary, a wide range of continental paleoclimate records from the inter-tropical zone provide a vivid picture of extraordinary hydroclimatic changes that occurred abruptly as the major areas of convection and subsidence across the region shifted in response to a disruption in the AMOC. The atmospheric response was swift and global in scale, resulting in significant hydroclimatic consequences across half of the earth's surface. Given their rapidity, these changes may have been far more consequential for the flora and fauna of the affected regions than the long-term changes resulting from the growth and decay of ice sheets.

9. Recommendations for Further Research

Although there is an impressive set of terrestrial proxies that provide evidence for major hydroclimatic changes across the tropics and sub-tropics (Figure 2), the network is sparse for events in MIS 3 and 4. This is an interesting period that contrasts with events in MIS2 in that boundary conditions were significantly different—most notably smaller continental ice sheets and higher sea-level in the earlier periods, which can affect the response of the atmospheric circulation to freshwater forcing (Kageyama et al., 2013). A better understanding of the source and distribution of freshwater is also needed, so that model simulations can move away from the ubiquitous hosing experiments in which freshwater is uniformly imposed (unrealistically) across the North Atlantic from 50°N to 70°N (cf. Roche et al., 2010). Modeling may help in understanding the movement of freshwater and associated IRD (e.g., Condron & Hill, 2021) and the magnitude and duration of AMOC disruption associated with different geographical patterns of freshwater forcing and model simulations that examine such differences are needed. There is a large spread in model AMOC response to freshwater forcing which means that relying on the results of a single model may not be the best strategy (Stouffer et al., 2006). Models are also commonly compared to pre-industrial conditions, rather than to conditions around the time of HEs, which means that they may not capture the additional effects of orbital and greenhouse gas forcing and ice sheet distribution. As much of the proxy evidence relating to THEs (and HEs) are isotopic records from stalagmites, the more widespread use of isotope-enabled models for paleoclimate simulations (for example, as carried out by Hu et al., 2019) would be a major step forward in more directly linking models and data.

Dating is an on-going issue for many proxy records, especially those from marine sediments. Indeed, as Table 1 illustrates, there is still considerable disagreement about the exact timing and duration of HEs in the

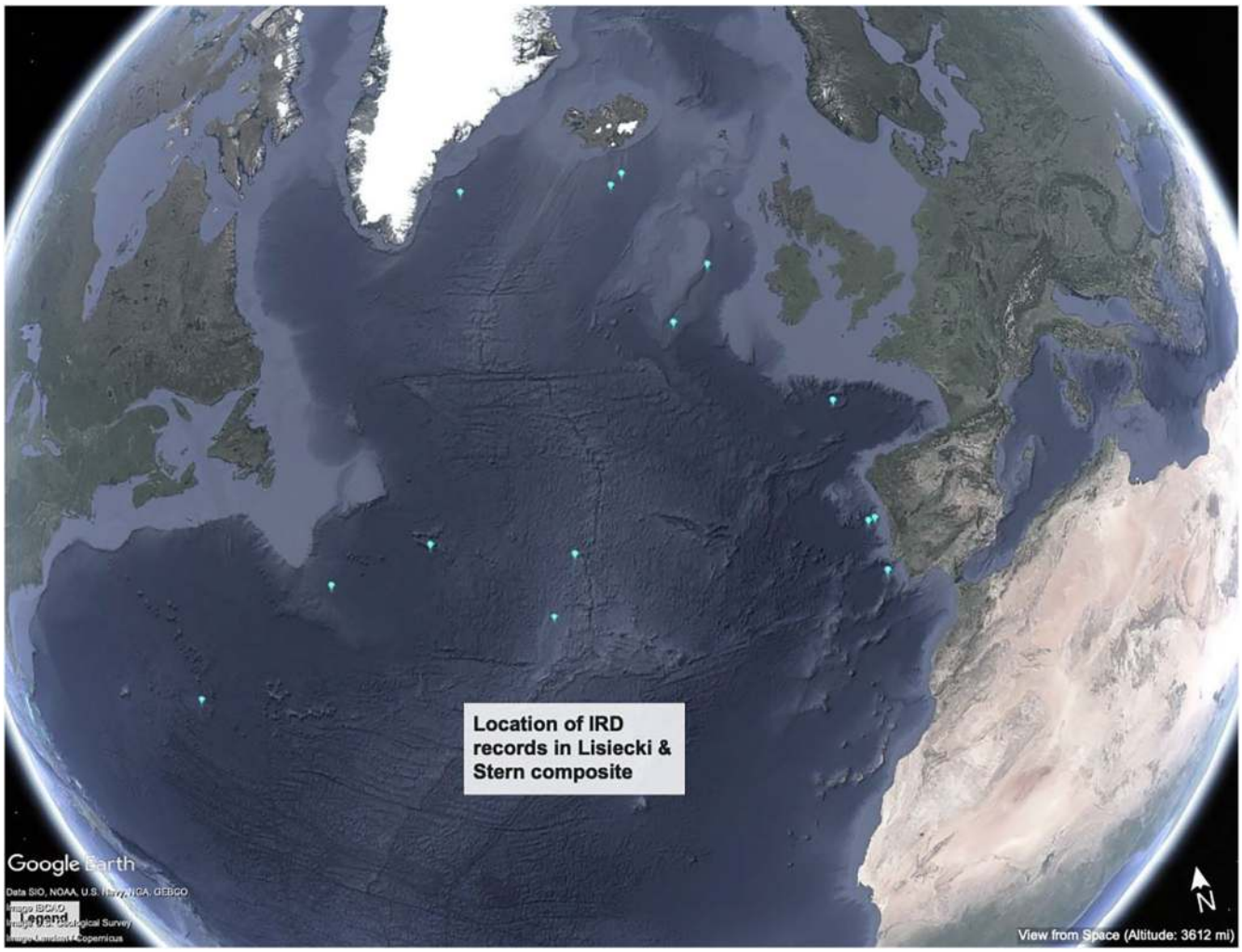

Figure 24. Location of IRD records used to produce a "stacked" composite time series (based on data provided in Lisiecki and Stern, 2016).

North Atlantic, especially in MIS3 and 4. Although we have used a stacked record of IRD throughout this article as a reference for freshwater forcing, the data therein is somewhat limited (Figure 24). It would be extremely useful to have a more comprehensive set of IRD records compiled using the best available dating control in order to better understand the timing and distribution of IRD, and whether there were phases of deposition within each HE event that were geographically widespread, as documented for a single site by Hodell et al. (2017). The best-dated terrestrial proxy records are from speleothems, and these currently provide a temporal framework for hydroclimatic events across South America and Asia, but there are, as yet, no comparable records from the African continent. There is also an on-going debate about the interpretation of $\delta^{18}O$ in speleothems simply in terms of rainfall amount (Hu et al., 2019; Lachniet, 2020). Ice core records of CH_4 provide extremely important evidence of wetland expansion (even though they do not indicate the geographical areas of such changes; Rhodes et al., 2015). Nevertheless, the additional chronological constraints on THEs that ice cores can provide is extremely important, especially for earlier THEs where dating is relatively poor.

Finally, the rapidity with which extreme hydroclimatic conditions began (and ended) in different geographical regions needs to be better resolved in time and space, by more widespread paleoclimatic records and many improved chronologies. The best-dated records (high-resolution speleothems) indicate that the changes in some locations were very abrupt (occurring in less than a few decades) and so it seems probable that the events we have described would have had profound consequences for the flora and fauna of the

tropics, affecting both resident and migratory species, as well people living in the region at the time. This topic seems well worth more detailed investigations.

Data Availability Statement

Data sources used in constructing the figures are indicated in each figure caption.

Acknowledgments
The authors thank Thomas C. Johnson, Martin Medina-Elizalde, and Alan Condron for insightful discussions and reviewers for their helpful comments and suggestions. This review developed from research on NSF grants PLR 1417667 and OPP-1744515, and prolonged COVID isolation. The authors declare no perceived or financial interests.

References

Andrews, J. T., & Voelker, A. H. (2018). "Heinrich events" (& sediments): A history of terminology and recommendations for future usage. *Quaternary Science Reviews*, *187*, 31–40. https://doi.org/10.1016/j.quascirev.2018.03.017

Arienzo, M. M., Swart, P. K., Broad, K., Clement, A. C., Pourmand, A., & Kakuk, B. (2017). Multi-proxy evidence of millennial climate variability from multiple Bahamian speleothems. *Quaternary Science Reviews*, *161*, 18–29. https://doi.org/10.1016/j.quascirev.2017.02.004

Arienzo, M. M., Swart, P. K., Pourmand, A., Broad, K., Clement, A., Murphy, L. N., et al. (2015). Bahamian speleothem reveals temperature decrease associated with Heinrich stadials. *Earth and Planetary Science Letters*, *430*, 377–386. https://doi.org/10.1016/j.epsl.2015.08.035

Arnold, T. E., Diefendorf, A. F., Brenner, M., Freeman, K. H., & Baczynski, A. A. (2018). Climate response of the Florida Peninsula to Heinrich events in the North Atlantic. *Quaternary Science Reviews*, *194*, 1–11. https://doi.org/10.1016/j.quascirev.2018.06.012

Arz, H. W., Pätzold, J., & Wefer, G. (1998). Correlated millennial-scale changes in surface hydrography and terrigenous sediment yield inferred from Last-Glacial marine deposits off Northeastern Brazil. *Quaternary Research*, *50*, 157–166. https://doi.org/10.1006/qres.1998.1992

Arz, H. W., Pätzold, J., & Wefer, G. (1999). The deglacial history of the western tropical Atlantic as inferred from high-resolution stable isotope records off northeastern Brazil. *Earth and Planetary Science Letters*, *167*, 105–117. https://doi.org/10.1016/s0012-821x(99)00025-4

Atwood, A. R., Donohoe, A., Battisti, D. S., Liu, X., & Pausata, F. S. (2020). Robust longitudinally variable responses of the ITCZ to a myriad of climate forcings. *Geophysical Research Letters*, *47*(17), e2020GL088833. https://doi.org/10.1029/2020gl088833

Ayliffe, L. K., Gagan, M. K., Zhao, J. X., Drysdale, R. N., Hellstrom, J. C., Hantoro, W. S., et al. (2013). Rapid interhemispheric climate links via the Australasian monsoon during the last deglaciation. *Nature Communications*, *4*(1), 1–6. https://doi.org/10.1038/ncomms3908

Baker, A. J., Sodemann, H., Baldini, J. U., Breitenbach, S. F., Johnson, K. R., van Hunen, J., & Zhang, P. (2015). Seasonality of westerly moisture transport in the East Asian summer monsoon and its implications for interpreting precipitation $\delta^{18}O$. *Journal of Geophysical Research: Atmospheres*, *120*(12), 5850–5862. https://doi.org/10.1002/2014jd022919

Baker, P. A., Rigsby, C. A., Seltzer, G. O., Fritz, S. C., Lowenstein, T. K., Bacher, N. P., & Veliz, C. (2001). Tropical climate changes at millennial and orbital timescales on the Bolivian Altiplano. *Nature*, *409*, 698–701. https://doi.org/10.1038/35055524

Bauska, T. K., Marcott, S. A., & Brook, E. J. (2021). Abrupt changes in the global carbon cycle during the last glacial period. *Nature Geoscience*, *14*(2), 91–96. https://doi.org/10.1038/s41561-020-00680-2

Behling, H., Arz, H. W., Pätzold, J., & Wefer, G. (2000). Late Quaternary vegetational and climate dynamics in northeastern Brazil, inferences from marine core GeoB 3104-1. *Quaternary Science Reviews*, *19*, 981–994. https://doi.org/10.1016/s0277-3791(99)00046-3

Berke, M. A., Johnson, T. C., Werne, J. P., Grice, K., Schouten, S., & Damsté, J. S. S. (2012). Molecular records of climate variability and vegetation response since the Late Pleistocene in the Lake Victoria basin, East Africa. *Quaternary Science Reviews*, *55*, 59–74. https://doi.org/10.1016/j.quascirev.2012.08.014

Blard, P. H., Sylvestre, F., Tripati, A. K., Claude, C., Causse, C., Coudrain, A., et al. (2011). Lake highstands on the Altiplano (Tropical Andes) contemporaneous with Heinrich 1 and the Younger Dryas: New insights from ^{14}C, U-Th dating, and $\delta^{18}O$ of carbonates. *Quaternary Science Reviews*, *30*, 3973–3989. https://doi.org/10.1016/j.quascirev.2011.11.001

Böhm, E. (2014). *Rekonstruktion der Atlantischen Zirkulation innerhalb des letzten Glazialen Zyklus*. Germany: Unpublished Doctoral dissertation, Faculty of Science and Mathematics, Ruprecht-Karls University.

Bouimetarhan, I., Prange, M., Schefuß, E., Dupont, L., Lippold, J., Mulitza, S., & Zonneveld, K. (2012). Sahel megadrought during Heinrich Stadial 1: Evidence for a three-phase evolution of the low-and mid-level West African wind system. *Quaternary Science Reviews*, *58*, 66–76. https://doi.org/10.1016/j.quascirev.2012.10.015

Bradley, R. S., & England, J. H. (2008). The Younger Dryas and the sea of ancient ice. *Quaternary Research*, *70*(1), 1–10. https://doi.org/10.1016/j.yqres.2008.03.002

Broccoli, A. J., Dahl, K. A., & Stouffer, R. J. (2006). Response of the ITCZ to Northern Hemisphere cooling. *Geophysical Research Letters*, *33*(1), L01702. https://doi.org/10.1029/2005GL024546

Broecker, W. S., Peteet, D. M., & Rind, D. (1985). Does the ocean-atmosphere system have more than one stable mode of operation? *Nature*, *315*, 21–26. https://doi.org/10.1038/315021a0

Brown, E. T., Johnson, T. C., Scholz, C. A., Cohen, A. S., & King, J. W. (2007). Abrupt change in tropical African climate linked to the bipolar seesaw over the past 55,000 yr. *Geophysical Research Letters*, *34*(20). https://doi.org/10.1029/2007gl031240

Burns, S. J., Fleitmann, D., Matter, A., Kramers, J., & Al-Subbary, A. A. (2003). Indian Ocean climate and an absolute chronology over Dansgaard/Oeschger events 9 to 13. *Science*, *301*(5638), 1365–1367. https://doi.org/10.1126/science.1086227

Burns, S. J., Fleitmann, D., Matter, A., Kramers, J., & Al-Subbary, A. A. (2004). Corrections and clarifications. *Science*, *305*, 1567.

Burrough, S. L., Thomas, D. S., & Bailey, R. M. (2009). Mega-Lake in the Kalahari: A Late Pleistocene record of the Palaeolake Makgadikgadi system. *Quaternary Science Reviews*, *28*(15–16), 1392–1411. https://doi.org/10.1016/j.quascirev.2009.02.007

Bush, M. B., & Colinvaux, P. A. (1990). A pollen record of a complete glacial cycle from lowland Panama. *Journal of Vegetation Science*, *1*, 105–118. https://doi.org/10.2307/3236060

Bush, M. B., Correa-Metrio, A., Hodell, D. A., Brenner, M., Anselmetti, F. S., Aristegui, D., et al. (2009). Re-evaluation of climate change in Lowland Central America during the Last Glacial Maximum using new sediment cores from Lake Petén Itzá, Guatemala. In F. Vimeux, F. Sylvestre, & M. Khodri (Eds.), *Past climate variability from the last glacial maximum to the Holocene in South America and surrounding regions* (pp. 113–128). Springer. https://doi.org/10.1007/978-90-481-2672-9_5

Cai, Y., An, Z., Cheng, H., Edwards, R. L., Kelly, M. J., Liu, W., et al. (2006). High-resolution absolute-dated Indian Monsoon record between 53 and 36 ka from Xiaobailong Cave, southwestern China. *Geology*, *34*, 621. https://doi.org/10.1130/g22567.1

Cai, Y., Fung, I. Y., Edwards, R. L., An, Z., Cheng, H., Lee, J. E., et al. (2015). Variability of stalagmite-inferred Indian monsoon precipitation over the past 252,000 yr. *Proceedings of the National Academy of Sciences*, *112*(10), 2954–2959. https://doi.org/10.1073/pnas.1424035112

Carolin, S. A., Cobb, K. M., Adkins, J. F., Clark, B., Conroy, J. L., Lejau, S., et al. (2013). Varied response of western Pacific hydrology to climate forcings over the last glacial period. *Science*, *340*(6140), 1564–1566. https://doi.org/10.1126/science.1233797

Channell, J. E., Hodell, D. A., Romero, O., Hillaire-Marcel, C., de Vernal, A., Stoner, J. S., et al. (2012). A 750 kyr detrital-layer stratigraphy for the North Atlantic (IODP sites U1302–U1303, Orphan Knoll, Labrador Sea). *Earth and Planetary Science Letters*, *317*, 218–230. https://doi.org/10.1016/j.epsl.2011.11.029

Chen, S., Wang, Y., Cheng, H., Edwards, R. L., Wang, X., Kong, X., & Liu, D. (2016). Strong coupling of Asian Monsoon and Antarctic climates on sub-orbital timescales. *Scientific Reports*, *6*, 32995. https://doi.org/10.1038/srep32995

Cheng, H., Edwards, R. L., Sinha, A., Spötl, C., Yi, L., Chen, S., et al. (2016). The Asian monsoon over the past 640,000 yr and ice age terminations. *Nature*, *534*, 640–646. https://doi.org/10.1038/nature18591

Cheng, H., Sinha, A., Cruz, F. W., Wang, X., Edwards, R. L., d'Horta, F. M., et al. (2013). Climate change patterns in Amazonia and biodiversity. *Nature Communications*, *4*(1), 1–6. https://doi.org/10.1038/ncomms2415

Cheng, H., Sinha, A., Wang, X., Cruz, F. W., & Edwards, R. L. (2012). The Global Paleomonsoon as seen through speleothem records from Asia and the Americas. *Climate Dynamics*, *39*(5), 1045–1062. https://doi.org/10.1007/s00382-012-1363-7

Cheng, H., Zhang, H., Zhao, J., Li, H., Ning, Y., & Kathayat, G. (2019). Chinese stalagmite paleoclimate researches: A review and perspective. *Science China Earth Sciences*, *62*, 1–25. https://doi.org/10.1007/s11430-019-9478-3

Cheng, W., Bitz, C. M., & Chiang, J. C. H. (2007). Adjustment of the global climate to an abrupt slowdown of the Atlantic meridional overturning circulation. In A. Schmittner, J. C. H. Chiang, & S. Hemming (Eds.), *Ocean circulation: Mechanisms and impacts—Past and future changes of meridional overturning. Geophysical Monograph 173* (pp. 295–313). Washington, D.C: American Geophysical UnionAGU. https://doi.org/10.1029/173gm19

Chiang, J. C. H., & Bitz, C. M. (2005). Influence of high latitude ice cover on the marine intertropical convergence zone. *Climate Dynamics*, *25*(5), 477–496. https://doi.org/10.1007/s00382-005-0040-5

Chiang, J. C. H., Cheng, W., & Bitz, C. M. (2008). Fast teleconnections to the tropical Atlantic sector from Atlantic thermohaline adjustment. *Geophysical Research Letters*, *35*, L07704. https://doi.org/10.1029/2008gl033292

Chiang, J. C. H., & Friedman, A. R. (2012). Extratropical cooling, interhemispheric thermal gradients, and tropical climate change. *Annual Reviews of Earth and Planetary Sciences*, *40*, 383–412. https://doi.org/10.1146/annurev-earth-042711-105545

Chiang, J. C. H., Fung, I. Y., Wu, C. H., Cai, Y., Edman, J. P., Liu, Y., et al. (2015). Role of seasonal transitions and westerly jets in East Asian paleoclimate. *Quaternary Science Reviews*, *108*, 111–129. https://doi.org/10.1016/j.quascirev.2014.11.009

Clemens, S. C., Holbourn, A., Kubota, Y., Lee, K. E., Liu, Z., Chen, G., et al. (2018). Precession-band variance missing from East Asian monsoon runoff. *Nature Communications*, *9*(1), 1–12. https://doi.org/10.1038/s41467-018-05814-0

Clement, A. C., Cane, M. A., & Seager, R. (2001). An orbitally driven tropical source for abrupt climate change. *Journal of Climate*, *14*, 2369–2375. https://doi.org/10.1175/1520-0442(2001)014<2369:aodtsf>2.0.co;2

Cohuo, S., Macario-González, L., Pérez, L., Sylvestre, F., Paillès, C., Curtis, J. H., et al. (2018). Climate ultrastructure and aquatic community response to Heinrich Stadials (HS5a-HS1) in the continental northern Neotropics. *Quaternary Science Reviews*, *197*, 75–91. https://doi.org/10.1016/j.quascirev.2018.07.015

Collins, J. A., Schefuß, E., Mulitza, S., Prange, M., Werner, M., Tharammal, T., et al. (2013). Estimating the hydrogen isotopic composition of past precipitation using leaf-waxes from western Africa. *Quaternary Science Reviews*, *65*, 88–101. https://doi.org/10.1016/j.quascirev.2013.01.007

Condron, A., & Hill, J. C. (2021). Timing of iceberg scours and massive ice-rafting events in the sub-tropical North Atlantic. *Nature Communications*, *12*, 3668–3681. https://doi.org/10.1038/s41467-021-23924-0

Condron, A., & Winsor, P. (2011). A subtropical fate awaited freshwater discharged from glacial Lake Agassiz. *Geophysical Research Letters*, *38*(3), L03705. https://doi.org/10.1029/2010GL046011

Condron, A., & Winsor, P. (2012). Meltwater routing and the Younger Dryas. *Proceedings of the National Academy of Sciences*, *109*(49), 19928–19933. https://doi.org/10.1073/pnas.1207381109

Correa-Metrio, A., Bush, M. B., Cabrera, K. R., Sully, S., Brenner, M., Hodell, D. A., et al. (2012). Rapid climate change and no-analog vegetation in lowland Central America during the last 86,000 yr. *Quaternary Science Reviews*, *38*, 63–75.

Correa-Metrio, A., Bush, M. B., Hodell, D. A., Brenner, M., Escobar, J., & Guilderson, T. (2012). The influence of abrupt climate change on the ice-age vegetation of the Central American lowlands. *Journal of Biogeography*, *39*, 497–509.

Corrick, E. C., Drysdale, R. N., Hellstrom, J. C., Capron, E., Rasmussen, S. O., Zhang, X., et al. (2020). Synchronous timing of abrupt climate changes during the last glacial period. *Science*, *369*, 963–969. https://doi.org/10.1126/science.aay5538

Cruz, F. W., Burns, S. J., Karmann, I., Sharp, W. D., & Vuille, M. (2006). Reconstruction of regional atmospheric circulation features during the late Pleistocene in subtropical Brazil from oxygen isotope composition of speleothems. *Earth and Planetary Science Letters*, *248*, 494–506. https://doi.org/10.1016/j.epsl.2006.06.019

Cruz, F. W., Vuille, M., Burns, S. J., Wang, X., Cheng, H., Werner, M., et al. (2009). Orbitally driven east-west antiphasing of South American precipitation. *Nature Geoscience*, *2*, 210–214. https://doi.org/10.1038/ngeo444

Denniston, R. F., Wyrwoll, K. H., Asmerom, Y., Polyak, V. J., Humphreys, W. F., Cugley, J., et al. (2013). North Atlantic forcing of millennial-scale Indo-Australian monsoon dynamics during the Last Glacial period. *Quaternary Science Reviews*, *72*, 159–168. https://doi.org/10.1016/j.quascirev.2013.04.012

Deplazes, G., Lückge, A., Peterson, L. C., Timmermann, A., Hamann, Y., Hughen, K. A., et al. (2013). Links between tropical rainfall and North Atlantic climate during the last glacial period. *Nature Geoscience*, *6*, 213–217. https://doi.org/10.1038/ngeo1712

Deplazes, G., Lückge, A., Stuut, J. B. W., Pätzold, J., Kuhlmann, H., Husson, D., et al. (2014). Weakening and strengthening of the Indian monsoon during Heinrich events and Dansgaard-Oeschger oscillations. *Paleoceanography*, *29*, 99–114. https://doi.org/10.1002/2013pa002509

Dong, B. W., & Sutton, R. T. (2002). Adjustment of the coupled ocean-atmosphere system to a sudden change in the thermohaline circulation. *Geophysical Research Letters*, *29*(15), 1728. https://doi.org/10.1029/2002GL015229

Donohoe, A., Marshall, J., Ferreira, D., & Mcgee, D. (2013). The relationship between ITCZ location and cross-equatorial atmospheric heat transport: From the seasonal cycle to the Last Glacial Maximum. *Journal of Climate*, *26*(11), 3597–3618. https://doi.org/10.1175/jcli-d-12-00467.1

Duan, F., Liu, D., Cheng, H., Wang, X., Wang, Y., Kong, X., & Chen, S. (2014). A high-resolution monsoon record of millennial-scale oscillations during Late MIS 3 from Wulu Cave, south-west China. *Journal of Quaternary Science*, *29*(1), 83–90. https://doi.org/10.1002/jqs.2681

Dung, N. C., Chen, Y. G., Chiang, H. W., Shen, C. C., Wang, X., Lam, D. D., et al. (2020). A decadal-resolution stalagmite record of strong Asian summer monsoon from Northwestern Vietnam over the Dansgaard-Oeschger events 2–4. *Journal of Asian Earth Sciences*, *3*, 100027.

Dupont, L. M., Schultz, F., Teboh Ewah, C., Jennerjahn, T. C., Paul, A., & Behling, H. (2010). Two-step vegetation response to enhanced precipitation in Northeast Brazil during Heinrich event 1. *Global Change Biology*, *16*, 1647–1660.
Dutt, S., Gupta, A. K., Clemens, S. C., Cheng, H., Singh, R. K., Kathayat, G., & Edwards, R. L. (2015). Abrupt changes in Indian summer monsoon strength during 33,800 to 5500 yr B.P. *Geophysical Research Letters*, *42*(13), 5526–5532. https://doi.org/10.1002/2015gl064015
Ehrmann, W., Schmiedl, G., Seidel, M., Krüger, S., & Schulz, H. (2016). A distal 140 kyr sediment record of Nile discharge and East African monsoon variability. *Climate of the Past*, *12*(3). https://doi.org/10.5194/cp-12-713-2016
Escobar, J., Hodell, D. A., Brenner, M., Curtis, J. H., Gilli, A., Mueller, A. D., et al. (2012). A ~43 ka record of paleoenvironmental change in the Central American lowlands inferred from stable isotopes of lacustrine ostracods. *Quaternary Science Reviews*, *37*, 92–104. https://doi.org/10.1016/j.quascirev.2012.01.020
Evans, J. L., & Webster, C. C. (2014). A variable sea surface temperature threshold for tropical convection. *Australian Meteorological and Oceanographic Journal*, *64*, S1–S8. https://doi.org/10.22499/2.6401.007
Fleitmann, D., & Matter, A. (2009). The speleothem record of climate variability in Southern Arabia. *Comptes Rendus Geoscience*, *341*(8–9), 633–642. https://doi.org/10.1016/j.crte.2009.01.006
Folkins, I., & Braun, C. (2003). Tropical rainfall and boundary layer moist entropy. *Journal of Climate*, *16*(11), 1807–1820. https://doi.org/10.1175/1520-0442(2003)016<1807:trablm>2.0.co;2
Gadgil, S. (2018). The monsoon system: Land-sea breeze or the ITCZ? *Journal of Earth System Science*, *127*(1), 1–29. https://doi.org/10.1007/s12040-017-0916-x
Gallego-Torres, D., Romero, O. E., Martínez-Ruiz, F., Kim, J. H., Donner, B., & Ortega-Huertas, M. (2014). Rapid bottom-water circulation changes during the last glacial cycle in the coastal low-latitude NE Atlantic. *Quaternary Research*, *81*(2), 330–338. https://doi.org/10.1016/j.yqres.2013.11.004
Garreaud, R., Vuille, M., Compagnucci, R., & Marengo, J. (2009). Present-day South American climate. *Paleogeography, Paleoclimatology, Paleoecology*, *281*, 180–195. https://doi.org/10.1016/j.palaeo.2007.10.032
Geen, R., Bordoni, S., Battisti, D. S., & Hui, K. (2020). Monsoons, ITCZ, and the concept of the global monsoon. *Reviews of Geophysics*, *58*, e2020RG00070. https://doi.org/10.1029/2020rg000700
Govil, P., & Naidu, P. D. (2011). Variations of Indian monsoon precipitation during the last 32 kyr reflected in the surface hydrography of the Western Bay of Bengal. *Quaternary Science Reviews*, *30*(27–28), 3871–3879. https://doi.org/10.1016/j.quascirev.2011.10.004
Graham, NE., & Barnett, T. P. (1987). Sea surface temperature, surface wind divergence, and convection over Tropical oceans. *Science*, *238*, 657–659. https://doi.org/10.1126/science.238.4827.657
Grauel, A.-L., Hodell, D. A., & Bernasconi, S. M. (2016). Quantitative estimates of tropical temperature change in lowland Central America during the last 42 ka. *Earth and Planetary Science Letters*, *438*, 37–46. https://doi.org/10.1016/j.epsl.2016.01.001
Grimm, E. C., Jacobson, G. L., Jr, Watts, W. A., Hansen, B. C. S., & Maasch, K. A. (1993). A 50,000 yr record of climate oscillations from Florida and its temporal correlation with the Heinrich events. *Science*, *261*, 198–200. https://doi.org/10.1126/science.261.5118.198
Grimm, E. C., Watts, W. A., Jacobsen, G. L., Hansen, B. C. S., Almquist, H. R., & Dieffenbacher-Krall, A. C. (2006). Evidence for warm wet Heinrich events in Florida. *Quaternary Science Reviews*, *25*, 2197–2211. https://doi.org/10.1016/j.quascirev.2006.04.008
Groot, M. H. M., Bogotá, R. G., Lourens, L. J., Hooghiemstra, H., Vriend, M., Berrio, J. C., et al. (2011). 14 other Fúquene Project MembersUltra-high resolution pollen record from the northern Andes reveals rapid shifts in montane climates within the last two glacial cycles. *Climates of the Past*, *7*, 299–316. https://doi.org/10.5194/cp-7-299-2011
Groot, M. H. M., Hooghiemstra, H., Berrio, J. C., & Giraldo, C. (2013). North Andean environmental and climatic change at orbital to sub-millennial time-scales: Vegetation, water levels, and sedimentary regimes from Lake Fúquene 130–27 ka. *Review of Palaeobotany and Paleoecology*, *197*, 186–204. https://doi.org/10.1016/j.revpalbo.2013.04.005
Guillevic, M., Bazin, L., Landais, A., Stowasser, C., Masson-Delmotte, V., Blunier, T., et al. (2014). Evidence for a three-phase sequence during Heinrich Stadial 4 using a multiproxy approach based on Greenland ice core records. *Climate of the Past*, *10*, 2115–2133. https://doi.org/10.5194/cp-10-2115-2014
Han, Z., Li, X., Yi, S., Stevens, T., Chen, Y., Wang, X., & Lu, H. (2015). Extreme monsoon aridity episodes recorded in South China during Heinrich Events. *Paleogeography, Paleoclimatology, Paleoecology*, *440*, 467–474. https://doi.org/10.1016/j.palaeo.2015.09.037
Held, I. M. (2001). The partitioning of the energy transport between the tropical ocean and atmosphere. *Journal of the Atmospheric Sciences*, *58*, 943–948. https://doi.org/10.1175/1520-0469(2001)058<0943:tpotpe>2.0.co;2
Hemming, S. (2004). Heinrich events: Massive late Pleistocene detritus layers of the North Atlantic and their global climate imprint. *Reviews of Geophysics*, *42*, RG1005. https://doi.org/10.1029/2003rg000128
Henry, L. G., McManus, J. F., Curry, W. B., Roberts, N. L., Piotrowski, A. M., & Keigwin, L. D. (2016). North Atlantic Ocean circulation and abrupt climate change during the last glaciation. *Science*, *353*(6298), 470–474. https://doi.org/10.1126/science.aaf5529
Hill, J. C., & Condron, A. (2014). Subtropical iceberg scours and meltwater routing in the deglacial western North Atlantic. *Nature Geoscience*, *7*(11), 806–810. https://doi.org/10.1038/ngeo2267
Hodell, D. A., Anselmetti, F. S., Ariztegui, D., Brenner, M., Curtis, J. H., Gilli, A., et al. (2008). An 85 ka record of climate change in lowland Central America. *Quaternary Science Reviews*, *27*, 1152–1165. https://doi.org/10.1016/j.quascirev.2008.02.008
Hodell, D. A., Channell, J. E., Curtis, J. H., Romero, O. E., & Röhl, U. (2008). Onset of "Hudson Strait" Heinrich events in the eastern North Atlantic at the end of the middle Pleistocene transition (~640 ka)? *Paleoceanography*, *23*(4), PA4218. https://doi.org/10.1029/2008PA001591
Hodell, D. A., Nicholl, J. A., Bontognali, T. R., Danino, S., Dorador, J., Dowdeswell, J. A., et al. (2017). Anatomy of Heinrich Layer 1 and its role in the last deglaciation. *Paleoceanography*, *32*(3), 284–303. https://doi.org/10.1002/2016pa003028
Hodell, D. A., Turchyn, A. V., Wiseman, C. J., Escobar, J., Curtis, J. H., Brenner, M., et al. (2012). Late Glacial temperature and precipitation changes in the lowland Neotropics by tandem measurement of $\delta^{18}O$ in biogenic carbonate and gypsum hydration water. *Geochimica et Cosmochimica Acta*, *77*, 352–368. https://doi.org/10.1016/j.gca.2011.11.026
Hooghiemstra, H. (1984). Vegetational and climatic history of the high plain of Bogotá, Colombia. In *Dissertationes Botanicae* (Vol. 79, p. 368). Vaduz: J. Cramer.
Hu, J., Emile-Geay, J., Tabor, C., Nusbaumer, J., & Partin, J. (2019). Deciphering oxygen isotope records from Chinese speleothems with an isotope-enabled climate model. *Paleoceanography and Paleoclimatology*, *34*(12), 2098–2112. https://doi.org/10.1029/2019pa003741
Huang, J., Wan, S., Li, A., & Li, T. (2019). Two-phase structure of tropical hydroclimate during Heinrich Stadial 1 and its global implications. *Quaternary Science Reviews*, *222*, 105900. https://doi.org/10.1016/j.quascirev.2019.105900
Hughen, K. A., & Heaton, T. J. (2020). Updated Cariaco Basin ^{14}C calibration dataset from 0 to 60 cal kyr B.P. *Radiocarbon*, *62*(4), 1001–1043. https://doi.org/10.1017/rdc.2020.53

Itambi, A. C., Von Dobeneck, T., Mulitza, S., Bickert, T., & Heslop, D. (2009). Millennial-scale northwest African droughts related to Heinrich events and Dansgaard-Oeschger cycles: Evidence in marine sediments from offshore Senegal. *Paleoceanography*, *24*, PA1205. https://doi.org/10.1029/2007pa001570

Jaeschke, A., Rühlemann, C., Arz, H., Heil, G., & Lohmann, G. (2007). Coupling of millennial-scale changes in sea surface temperature and precipitation off northeastern Brazil with high latitude climate shifts during the last glacial period. *Paleoceanography*, *22*. https://doi.org/10.1029/2006PA001391.2007

Jennerjahn, T. C., Ittekkot, V., Arz, H. W., Behling, H., Pätzold, J., & Wefer, G. (2004). Asynchronous terrestrial marine signals of climate change during Heinrich events. *Science*, *306*, 2236–2239. https://doi.org/10.1126/science.1102490

Jiang, X., He, Y., Shen, C. C., Lee, S. Y., Yang, B., Lin, K., & Li, Z. (2014). Decoupling of the East Asian summer monsoon and Indian summer monsoon between 20 and 17 ka. *Quaternary Research*, *82*(1), 146–153. https://doi.org/10.1016/j.yqres.2014.05.001

Jullien, E., Grousset, F., Malaizé, B., Duprat, J., Sanchez-Goni, M. F., Eynaud, F., et al. (2007). Low-latitude "dusty events" vs. high-latitude "icy Heinrich events". *Quaternary Research*, *68*(3), 379–386. https://doi.org/10.1016/j.yqres.2007.07.007

Just, J., Dekkers, M. J., von Dobeneck, T., van Hoesel, A., & Bickert, T. (2012). Signatures and significance of aeolian, fluvial, bacterial and diagenetic magnetic mineral fractions in late Quaternary marine sediments off Gambia, NW Africa. *Geochemistry, Geophysics, Geosystems*, *13*(9). https://doi.org/10.1029/2012gc004146

Just, J., Schefuß, E., Kuhlmann, H., Stuut, J. B. W., & Pätzold, J. (2014). Climate induced sub-basin source-area shifts of Zambezi River sediments over the past 17 ka. *Paleogeography, Paleoclimatology, Paleoecology*, *410*, 190–199. https://doi.org/10.1016/j.palaeo.2014.05.045

Kageyama, M., Merkel, U., Otto-Bliesner, B., Prange, M., Abe-Ouchi, A., Lohmann, G., et al. (2013). Climatic impacts of fresh water hosing under Last Glacial Maximum conditions: A multi-model study. *Climate of the Past*, *9*(2), 935–953. https://doi.org/10.5194/cp-9-935-2013

Kanner, L. C., Burns, S. J., Cheng, H., & Edwards, R. L. (2012). High-latitude forcing of the South American summer monsoon during the Last Glacial. *Science*, *335*, 570–573. https://doi.org/10.1126/science.1213397

Kathayat, G., Cheng, H., Sinha, A., Spötl, C., Edwards, R. L., Zhang, H., et al. (2016). Indian monsoon variability on millennial-orbital timescales. *Scientific Reports*, *6*, 24374. https://doi.org/10.1038/srep24374

Kaufman, L. S., Chapman, L. J., & Chapman, C. A. (1997). Evolution in fast forward: Haplochromine fishes of the Lake Victoria region. *Endeavour*, *21*(1), 23–30. https://doi.org/10.1016/s0160-9327(96)10034-x

Kaushal, N., Breitenbach, S. F., Lechleitner, F. A., Sinha, A., Tewari, V. C., Ahmad, S. M., et al. (2018). The Indian summer monsoon from a speleothem $\delta^{18}O$ perspective—A review. *Quaternary*, *1*(3), 29. https://doi.org/10.3390/quat1030029

Kim, J. H., Schneider, R. R., Mulitza, S., & Müller, P. J. (2003). Reconstruction of SE trade-wind intensity based on sea-surface temperature gradients in the Southeast Atlantic over the last 25 kyr. *Geophysical Research Letters*, *30*(22). https://doi.org/10.1029/2003gl017557

Kissel, C. (2005). Magnetic signature of rapid climatic variations in glacial North Atlantic, a review. *Comptes Rendus Geoscience*, *337*(10–11), 908–918. https://doi.org/10.1016/j.crte.2005.04.009

Knutti, R., Flückiger, J., Stocker, T. F., & Timmermann, A. (2004). Strong hemispheric coupling of glacial climate through freshwater discharge and ocean circulation. *Nature*, *430*(7002), 851–856. https://doi.org/10.1038/nature02786

Lachniet, M. S. (2020). Illuminating the meaning of Asian monsoon cave speleothem records. *Paleoceanography and Paleoclimatology*, *35*, e2019PA003841. https://doi.org/10.1029/2019pa003841

Lachniet, M. S., Johnson, L., Asmerom, Y., Burns, S. J., Polyak, V., Patterson, W. P., et al. (2009). Late Quaternary moisture export across Central America and to Greenland: Evidence for tropical rainfall variability from Costa Rican stalagmites. *Quaternary Science Reviews*, *28*, 3348–3360. https://doi.org/10.1016/j.quascirev.2009.09.018

Lamb, H. F., Bates, C. R., Coombes, P. V., Marshall, M. H., Umer, M., Davies, S. J., & Dejen, E. (2007). Late Pleistocene desiccation of Lake Tana, source of the Blue Nile. *Quaternary Science Reviews*, *26*(3–4), 287–299. https://doi.org/10.1016/j.quascirev.2006.11.020

Lebamba, J., Vincens, A., & Maley, J. (2012). Pollen, vegetation change, and climate at Lake Barombi Mbo (Cameroon) during the last ca. 33,000 cal yr B.P: A numerical approach. *Climate of the Past*, *8*(1), 59–78. https://doi.org/10.5194/cp-8-59-2012

Lézine, A. M., Assi-Kaudjhis, C., Roche, E., Vincens, A., & Achoundong, G. (2013). Towards an understanding of West African montane forest response to climate change. *Journal of Biogeography*, *40*(1), 183–196. https://doi.org/10.1111/j.1365-2699.2012.02770.x

Lézine, A. M., Izumi, K., Kageyama, M., & Achoundong, G. (2019). A 90,000 yr record of Afromontane forest responses to climate change. *Science*, *363*(6423), 177–181. https://doi.org/10.1126/science.aav6821

Li, C., Battisti, D. S., Schrag, D. P., & Tziperman, E. (2005). Abrupt climate shifts in Greenland due to displacements of the sea ice edge. *Geophysical Research Letters*, *32*(19), L19702. https://doi.org/10.1029/2005gl023492

Li, T., Shen, C., Li, H., Li, J., Chiang, H., Song, S., et al. (2011). Oxygen and carbon isotopic systematics of aragonite speleothems and water in Furong Cave, Chongqing, China. *Geochimica et Cosmochimica Acta*, *75*, 4140–4156. https://doi.org/10.1016/j.gca.2011.04.003

Li, T., Yuan, D., Li, H., Yang, Y., Wang, J., Wang, X., et al. (2007). High-resolution climate variability of southwest China during 57–70 ka reflected in a stalagmite $\delta^{18}O$ record from Xinya Cave. *Science in China Series D: Earth Sciences*, *50*(8), 1202–1208. https://doi.org/10.1007/s11430-007-0059-z

Liang, Y., Zhao, K., Edwards, R. L., Wang, Y., Shao, Q., Zhang, Z., et al. (2020). East Asian monsoon changes early in the last deglaciation and insights into the interpretation of oxygen isotope changes in the Chinese stalagmite record. *Quaternary Science Reviews*, *250*, 106699. https://doi.org/10.1016/j.quascirev.2020.106699

Lippold, J., Grützner, J., Winter, D., Lahaye, Y., Mangini, A., & Christl, M. (2009). Does sedimentary $^{231}Pa/^{230}Th$ from the Bermuda Rise monitor past Atlantic meridional overturning circulation? *Geophysical Research Letters*, *36*(12), L12601. https://doi.org/10.1029/2009gl038068

Lisiecki, L. E., & Stern, J. V. (2016). Regional and global benthic $\delta^{18}O$ stacks for the last glacial cycle. *Paleoceanography*, *31*, 1368–1394. https://doi.org/10.1002/2016pa003002

Liu, D., Wang, Y., Cheng, H., Edwards, R. L., Kong, X., Wang, X., et al. (2010). Sub-millennial variability of Asian monsoon intensity during the early MIS 3 and its analog to the ice age terminations. *Quaternary Science Reviews*, *29*(9–10), 1107–1115. https://doi.org/10.1016/j.quascirev.2010.01.008

Maher, B. A., & Thompson, R. (2012). Oxygen isotopes from Chinese caves: Records not of monsoon rainfall but of circulation regime. *Journal of Quaternary Science*, *27*(6), 615–624. https://doi.org/10.1002/jqs.2553

Mamalakis, A., Randerson, J. T., Yu, J. Y., Pritchard, M. S., Magnusdottir, G., Smyth, P., et al. (2021). Zonally contrasting shifts of the tropical rain belt in response to climate change. *Nature Climate Change*, 1–9. https://doi.org/10.1038/s41558-020-00963-x

Marshall, M. H., Lamb, H. F., Huws, D., Davies, S. J., Bates, R., Bloemendal, J., et al. (2011). Late Pleistocene and Holocene drought events at Lake Tana, the source of the Blue Nile. *Global and Planetary Change*, *78*(3–4), 147–161. https://doi.org/10.1016/j.gloplacha.2011.06.004

Martrat, B., Grimalt, J. O., Shackleton, N. J., de Abreu, L., Hutterli, M. A., & Stocker, T. F. (2007). Four climate cycles of recurring deep and surface water destabilizations on the Iberian margin. *Science*, *317*(5837), 502–507. https://doi.org/10.1126/science.1139994

Mays, J. L., Brenner, M., Curtis, J. H., Curtis, K. V., Hodell, D. A., Correa-Metrio, A., et al. (2017). Stable carbon isotopes ($\delta^{13}C$) of total organic carbon and long-chain n-alkanes as proxies for climate and environmental change in a sediment core from Lake Petén-Itzá, Guatemala. *Journal of Paleolimnology*, *57*, 307–319. https://doi.org/10.1007/s10933-017-9949-z

McGee, D., Donohoe, A., Marshall, J., & Ferreira, D. (2014). Changes in ITCZ location and cross-equatorial heat transport at the Last Glacial Maximum, Heinrich Stadial 1, and the mid-Holocene. *Earth and Planetary Science Letters*, *390*, 69–79. https://doi.org/10.1016/j.epsl.2013.12.043

McManus, J. F., Francois, R., Gherardi, J.-M., Keigwin, L. D., & Brown-Leger, S. (2004). Collapse and rapid resumption of Atlantic meridional circulation linked to deglacial climate changes. *Nature*, *428*(6958), 834–837. https://doi.org/10.1038/nature02494

McManus, J. F., Oppo, D. W., & Cullen, J. L. (1999). A 0.5 Myr record of millennial-scale climate variability in the North Atlantic. *Science*, *283*(5404), 971–975. https://doi.org/10.1126/science.283.5404.971

Medina-Elizalde, M., Burns, S. J., Polanco-Martinez, J., Lases-Hernández, F., Bradley, R., Wang, H. C., & Shen, C. C. (2017). Synchronous precipitation reduction in the American Tropics associated with Heinrich 2. *Scientific Reports*, *7*(1), 1–12. https://doi.org/10.1038/s41598-017-11742-8

Moernaut, J., Verschuren, D., Charlet, F., Kristen, I., Fagot, M., & De Batist, M. (2010). The seismic-stratigraphic record of lake-level fluctuations in Lake Challa: Hydrological stability and change in equatorial East Africa over the last 140 kyr. *Earth and Planetary Science Letters*, *290*(1–2), 214–223. https://doi.org/10.1016/j.epsl.2009.12.023

Mohtadi, M., Prange, M., Oppo, D. W., De Pol-Holz, R., Merkel, U., Zhang, X., et al. (2014). North Atlantic forcing of tropical Indian Ocean climate. *Nature*, *509*(7498), 76–80. https://doi.org/10.1038/nature13196

Mollier-Vogel, E., Leduc, G., Böschen, T., Martinez, P., & Schneider, R. R. (2013). Rainfall response to orbital and millennial forcing in northern Peru over the last 19 ka. *Quaternary Science Reviews*, *76*, 29–38. https://doi.org/10.1016/j.quascirev.2013.06.021

Mosblech, N. A. S., Bush, M. B., Gosling, W. D., Hodell, D., Thomas, L., van Calsteren, P., et al. (2012). North Atlantic forcing of Amazonian precipitation during the last ice age. *Nature Geoscience*, *5*, 817–820. https://doi.org/10.1038/ngeo1588

Mulitza, S., Prange, M., Stuut, J. B., Zabel, M., Von Dobeneck, T., Itambi, A. C., et al. (2008). Sahel megadroughts triggered by glacial slowdowns of Atlantic meridional overturning. *Paleoceanography*, *23*(4). https://doi.org/10.1029/2008pa001637

Muller, J., Kylander, M., Wüst, R. A., Weiss, D., Martinez-Cortizas, A., LeGrande, A. N., et al. (2008). Possible evidence for wet Heinrich phases in tropical NE Australia: The Lynch's Crater deposit. *Quaternary Science Reviews*, *27*(5–6), 468–475. https://doi.org/10.1016/j.quascirev.2007.11.006

Muller, J., McManus, J. F., Oppo, D. W., & Francois, R. (2012). Strengthening of the Northeast Monsoon over the Flores Sea, Indonesia, at the time of Heinrich event 1. *Geology*, *40*(7), 635–638. https://doi.org/10.1130/g32878.1

Munday, C., Washington, R., & Hart, N. (2021). African Low-Level Jets and Their Importance for Water Vapor Transport and Rainfall. *Geophysical Research Letters*, *48*(1), e2020GL090999. https://doi.org/10.1029/2020gl090999

Nace, T. E., Baker, P. A., Dwyer, G. S., Silva, C. G., Rigsby, C. A., Burns, S. J., et al. (2014). The role of North Brazil Current transport in the paleoclimate of the Brazilian Nordeste margin and paleoceanography of the western tropical Atlantic during the late Quaternary. *Paleogeography, Paleoclimatology, Paleoecology*, *415*, 3–13. https://doi.org/10.1016/j.palaeo.2014.05.030

Ng, H. C., Robinson, L. F., McManus, J. F., Mohamed, K. J., Jacobel, A. W., Ivanovic, R. F., et al. (2018). Coherent deglacial changes in western Atlantic Ocean circulation. *Nature Communications*, *9*(1), 1–10. https://doi.org/10.1038/s41467-018-05312-3

Nicholson, S. E. (2018). The ITCZ and the seasonal cycle over equatorial Africa. *Bulletin of the American Meteorological Society*, *99*(2), 337–348. https://doi.org/10.1175/bams-d-16-0287.1

Nicholson, S. E., & Grist, J. P. (2003). The seasonal evolution of the atmospheric circulation over West Africa and equatorial Africa. *Journal of Climate*, *16*(7), 1013–1030. https://doi.org/10.1175/1520-0442(2003)016<1013:tseota>2.0.co;2

Niedermeyer, E. M., Schefuß, E., Sessions, A. L., Mulitza, S., Mollenhauer, G., Schulz, M., & Wefer, G. (2010). Orbital-and millennial-scale changes in the hydrologic cycle and vegetation in the western African Sahel: Insights from individual plant wax δD and $\delta^{13}C$. *Quaternary Science Reviews*, *29*(23–24), 2996–3005. https://doi.org/10.1016/j.quascirev.2010.06.039

Nunnery, J. A. (2012). *A reconstruction of precipitation and hydrologic variability on the Peruvian and Bolivian Altiplano during the late Quaternary*, (Unpublished Ph.D. thesis). (pp. 185). Department of Earth and Ocean Sciences, Duke University.

Partin, J. W., Cobb, K. M., Adkins, J. F., Clark, B., & Fernandez, D. P. (2007). Millennial-scale trends in west Pacific warm pool hydrology since the Last Glacial Maximum. *Nature*, *449*(7161), 452–455. https://doi.org/10.1038/nature06164

Patiño, L., Velez, M. I., Weber, M., Velásquez-r, C. A., David, S., Rueda, M., et al. (2020). Late Pleistocene-Holocene environmental and climatic history of a freshwater paramo ecosystem in the northern Andes. *Journal of Quaternary Science*, *35*(8), 1046–1056. https://doi.org/10.1002/jqs.3249

Pausata, F. S., Battisti, D. S., Nisancioglu, K. H., & Bitz, C. M. (2011). Chinese stalagmite $\delta^{18}O$ controlled by changes in the Indian monsoon during a simulated Heinrich event. *Nature Geoscience*, *4*, 474–480. https://doi.org/10.1038/ngeo1169

Peck, J. A., Green, R. R., Shanahan, T., King, J. W., Overpeck, J. T., & Scholz, C. A. (2004). A magnetic mineral record of late Quaternary tropical climate variability from Lake Bosumtwi, Ghana. *Paleogeography, Paleoclimatology, Paleoecology*, *215*(1–2), 37–57. https://doi.org/10.1016/s0031-0182(04)00438-9

Perez, L., Correa-Metrio, A., Cohuo, S., González, L. M., Echeverria-Galindo, P., Brenner, M., et al. (2021). Ecological turnover in neotropical freshwater and terrestrial communities during episodes of abrupt climate change. *Quaternary Research*, *101*, 26–36. https://doi.org/10.1017/qua.2020.124

Peterson, L. C., Haug, G. H., Hughen, K. A., & Röhl, U. (2000). Rapid changes in the hydrologic cycle of the tropical Atlantic during the last glacial. *Science*, *290*, 1947–1951. https://doi.org/10.1126/science.290.5498.1947

Peterson, L. C., Overpeck, J. T., Kipp, N. G., & Imbrie, J. (1991). A high-resolution late Quaternary upwelling record from the anoxic Cariaco Basin, Venezuela. *Paleoceanography*, *6*, 99–119. https://doi.org/10.1029/90pa02497

Placzek, C. J., Quade, J., & Patchett, P. J. (2013). A 130 ka reconstruction of rainfall on the Bolivian Altiplano. *Earth and Planetary Science Letters*, *363*, 97–108. https://doi.org/10.1016/j.epsl.2012.12.017

Rashid, H., England, E., Thompson, L., & Polyak, L. (2011). Late glacial to Holocene Indian summer monsoon variability based upon sediment records taken from the Bay of Bengal. *Terrestrial, Atmospheric and Oceanic Sciences*, *22*(2), 215–228. https://doi.org/10.3319/tao.2010.09.17.02(tibxs)

Rhodes, R. H., Brook, E. J., Chiang, J. C., Blunier, T., Maselli, O. J., McConnell, J. R., et al. (2015). Enhanced tropical methane production in response to iceberg discharge in the North Atlantic. *Science*, *348*(6238), 1016–1019. https://doi.org/10.1126/science.1262005

Roberts, W. H. G., Valdes, P. J., & Singarayer, J. S. (2017). Can energy fluxes be used to interpret glacial/interglacial precipitation changes in the tropics? *Geophysical Research Letters*, *44*, 6373–6382. https://doi.org/10.1002/2017gl073103

Roche, D. M., Wiersma, A. P., & Renssen, H. (2010). A systematic study of the impact of freshwater pulses with respect to different geographical locations. *Climate Dynamics*, *34*(7), 997–1013. https://doi.org/10.1007/s00382-009-0578-8
Rühlemann, C., Mulitza, S., Müller, P. J., Wefer, G., & Zahn, R. (1999). Warming of the tropical Atlantic Ocean and slowdown of thermohaline circulation during the last deglaciation. *Nature*, *402*, 511–514. https://doi.org/10.1038/990069
Sachs, J. P., & Lehman, S. J. (1999). Subtropical North Atlantic temperatures 60,000–30,000 yr ago. *Science*, *286*, 756–759. https://doi.org/10.1126/science.286.5440.756
Sanchez Goñi, M. F., & Harrison, S. P. (2010). Millennial-scale climate variability and vegetation changes during the Last Glacial: Concepts and terminology. *Quaternary Science Reviews*, *29*(21–22), 2823–2827. https://doi.org/10.1016/j.quascirev.2009.11.014
Schefuß, E., Kuhlmann, H., Mollenhauer, G., Prange, M., & Pätzold, J. (2011). Forcing of wet phases in southeast Africa over the past 17,000 yr. *Nature*, *480*, 509–512. https://doi.org/10.1038/nature10685
Schefuß, E., Schouten, S., & Schneider, R. R. (2005). Climatic controls on central African hydrology during the past 20,000 yr. *Nature*, *437*(7061), 1003–1006. https://doi.org/10.1038/nature03945
Schneider, T., Bischoff, T., & Haug, G. H. (2014). Migrations and dynamics of the intertropical convergence zone. *Nature*, *513*(7516), 45–53. https://doi.org/10.1038/nature13636
Seager, R., & Battisti, D. S. (2007). Challenges to our understanding of the general circulation: Abrupt climate change. In T. Schneider, & A. H. Sobel (Eds.), *Global circulation of the atmosphere* (pp. 332–372). Princeton, N.J: Princeton Univ. Press.
Seager, R., Battisti, D. S., Yin, J., Gordon, N., Naik, N., Clement, A. C., & Cane, M. A. (2002). Is the Gulf Stream responsible for Europe's mild winters? *Quarterly Journal of the Royal Meteorological Society*, *128*(586), 2563–2586. https://doi.org/10.1256/qj.01.128
Seehausen, O. (2002). Patterns in fish radiation are compatible with Pleistocene desiccation of Lake Victoria and 14,600 yr history for its cichlid species flock. *Proceedings of the Royal Society of London. Series B: Biological Sciences*, *269*(1490), 491–497. https://doi.org/10.1098/rspb.2001.1906
Shakun, J. D., Burns, S. J., Fleitmann, D., Kramers, J., Matter, A., & Al-Subary, A. (2007). A high-resolution, absolute-dated deglacial speleothem record of Indian Ocean climate from Socotra Island, Yemen. *Earth and Planetary Science Letters*, *259*, 442–456. https://doi.org/10.1016/j.epsl.2007.05.004
Shanahan, T. M., Beck, J. W., Overpeck, J. T., McKay, N. P., Pigati, J. S., Peck, J. A., et al. (2012). Late Quaternary sedimentological and climate change at Lake Bosumtwi Ghana: New constraints from laminae analysis and radiocarbon age modeling. *Paleogeography, Paleoclimatology, Paleoecology*, *361*, 49–60. https://doi.org/10.1016/j.palaeo.2012.08.001
Shiau, L. J., Chen, M. T., Clemens, S. C., Huh, C. A., Yamamoto, M., & Yokoyama, Y. (2011). Warm pool hydrological and terrestrial variability near southern Papua New Guinea over the past 50 k. *Geophysical Research Letters*, *38*, L00F01. https://doi.org/10.1029/2010GL045309
Singarayer, J. S., & Burrough, S. L. (2015). Interhemispheric dynamics of the African rain belt during the late Quaternary. *Quaternary Science Reviews*, *124*, 48–67. https://doi.org/10.1016/j.quascirev.2015.06.021
Singarayer, J. S., Valdes, P. J., & Roberts, W. H. (2017). Ocean dominated expansion and contraction of the late Quaternary tropical rain belt. *Scientific Reports*, *7*(1), 1–9. https://doi.org/10.1038/s41598-017-09816-8
Stager, J. C., Mayewski, P. A., & Meeker, L. D. (2002). Cooling cycles, Heinrich events, and the desiccation of Lake Victoria. *Paleogeography, Paleoclimatology, Paleoecology*, *183*, 169–178. https://doi.org/10.1016/s0031-0182(01)00468-0
Stager, J. C., Ryves, D. B., Chase, B. M., & Pausata, F. S. R. (2011). Catastrophic drought in the Afro-Asian monsoon region during Heinrich Event 1. *Science*, *331*, 1299–1302. https://doi.org/10.1126/science.1198322
Stouffer, R. J., Yin, J., Gregory, J. M., Dixon, K. W., Spelman, M. J., Hurlin, W., et al. (2006). Investigating the causes of the response of the thermohaline circulation to past and future climate changes. *Journal of Climate*, *19*(8), 1365–1387. https://doi.org/10.1175/jcli3689.1
Stríkis, N. M., Chiessi, C. M., Cruz, F. W., Vuille, M., Cheng, H., de Souza Barreto, E. A., et al. (2015). Timing and structure of Mega-SACZ events during Heinrich Stadial 1. *Geophysical Research Letters*, *42*(13), 5477–5484A. https://doi.org/10.1002/2015gl064048
Stríkis, N. M., Cruz, F. W., Barreto, E. A., Naughton, F., Vuille, M., Cheng, H., et al. (2018). South American monsoon response to iceberg discharge in the North Atlantic. *Proceedings of the National Academy of Sciences*, *115*(15), 3788–3793. https://doi.org/10.1073/pnas.1717784115
Thomas, D. S., Bailey, R., Shaw, P. A., Durcan, J. A., & Singarayer, J. S. (2009). Late Quaternary highstands at Lake Chilwa, Malawi: Frequency, timing and possible forcing mechanisms in the last 44 ka. *Quaternary Science Reviews*, *28*(5–6), 526–539. https://doi.org/10.1016/j.quascirev.2008.10.023
Thomas, D. S., Burrough, S. L., & Parker, A. G. (2012). Extreme events as drivers of early human behavior in Africa? The case for variability, not catastrophic drought. *Journal of Quaternary Science*, *27*(1), 7–12. https://doi.org/10.1002/jqs.1557
Thompson, L. G., Mosley-Thompson, E., & Henderson, K. A. (2000). Ice-core palaeoclimate records in tropical South America since the Last Glacial Maximum. *Journal of Quaternary Science*, *15*(4), 377–394. https://doi.org/10.1002/1099-1417(200005)15:4<377::aid-jqs542>3.0.co;2-l
Tierney, J. E., Pausata, F. S., & Demenocal, P. (2016). Deglacial Indian monsoon failure and North Atlantic stadials linked by Indian Ocean surface cooling. *Nature Geoscience*, *9*(1), 46–50. https://doi.org/10.1038/ngeo2603
Tierney, J. E., Russell, J. M., Damsté, J. S. S., Huang, Y., & Verschuren, D. (2011). Late Quaternary behavior of the East African monsoon and the importance of the Congo Air Boundary. *Quaternary Science Reviews*, *30*(7–8), 98–807. https://doi.org/10.1016/j.quascirev.2011.01.017
Tierney, J. E., Russell, J. M., Huang, Y., Damsté, J. S. S., Hopmans, E. C., & Cohen, A. S. (2008). Northern hemisphere controls on tropical southeast African climate during the past 60,000 yr. *Science*, *322*(5899), 252–255. https://doi.org/10.1126/science.1160485
Tjallingii, R., Claussen, M., Stuut, J. B. W., Fohlmeister, J., Jahn, A., Bickert, T., et al. (2008). Coherent high-and low-latitude control of the northwest African hydrological balance. *Nature Geoscience*, *1*(10), 670–675. https://doi.org/10.1038/ngeo289
Torres, V., Hooghiemstra, H., Lourens, L., & Tzedakis, P. C. (2013). Astronomical tuning of long pollen records reveals the dynamic history of montane biomes and lake levels in the tropical high Andes during the Quaternary. *Quaternary Science Reviews*, *63*, 59–72. https://doi.org/10.1016/j.quascirev.2012.11.004
Trenberth, K. E., & Caron, J. M. (2001). Estimates of meridional atmosphere and ocean heat transports. *Journal of Climate*, *14*(16), 3433–3443. https://doi.org/10.1175/1520-0442(2001)014<3433:eomaao>2.0.co;2
van Beynen, P., Polk, J. S., Asmerom, Y., & Polyak, V. (2017). Late Pleistocene and mid-Holocene climate change derived from a Florida speleothem. *Quaternary International*, *449*, 5–82. https://doi.org/10.1016/j.quaint.2017.05.008
van der Lubbe, H. J. L., Frank, M., Tjallingii, R., & Schneider, R. R. (2016). Neodymium isotope constraints on provenance, dispersal, and climate-driven supply of Zambezi sediments along the Mozambique Margin during the past ~45,000 yr. *Geochemistry, Geophysics, Geosystems*, *17*(1), 181–198. https://doi.org/10.1002/2015gc006080
Velásquez-R, C. A., & Hooghiemstra, H. (2013). Pollen-based 17 kyr forest dynamics and climate change from the Western Cordillera of Colombia; no-analog associations and temporarily lost biomes. *Review of Palaeobotany and Palynology*, *194*, 38–49. https://doi.org/10.1016/j.revpalbo.2013.03.001

Vellinga, M., & Wood, R. A. (2002). Global climatic impacts of a collapse of the Atlantic thermohaline circulation. *Climatic Change*, *54*(3), 251–267. https://doi.org/10.1023/a:1016168827653

Walczak, M. H., Mix, A. C., Cowan, E. A., Fallon, S., Fifield, L. K., Alder, J. R., et al. (2020). Phasing of millennial-scale climate variability in the Pacific and Atlantic Oceans. *Science*, *370*(6517), 716–720. https://doi.org/10.1126/science.aba7096

Wang, X., Auler, A. S., Edwards, R. L., Cheng, H., Cristall, P. S., Smart, P., et al. (2004). Wet periods in northeastern Brazil over the past 210 kyr linked to distant climate anomalies. *Nature*, *432*, 740–743. https://doi.org/10.1038/nature03067

Wang, X., Auler, A. S., Edwards, R. L., Cheng, H., Ito, E., & Solheid, M. (2006). Interhemispheric anti-phasing of rainfall during the last glacial period. *Quaternary Science Reviews*, *25*, 3391–3403. https://doi.org/10.1016/j.quascirev.2006.02.009

Wang, Y., Cheng, H., Edwards, R., An, Z., Wu, J., Shen, C., & Dorale, J. (2001). A high-resolution absolute-dated late Pleistocene monsoon record from Hulu Cave, China. *Science*, *294*, 2345–2348. https://doi.org/10.1126/science.1064618

Warken, S. F., Scholz, D., Spötl, C., Jochum, K. P., Pajón, J. M., Bahr, A., & Mangini, A. (2019). Caribbean hydroclimate and vegetation history across the last glacial period. *Quaternary Science Reviews*, *218*, 75–90. https://doi.org/10.1016/j.quascirev.2019.06.019

Warken, S. F., Vieten, R., Winter, A., Spötl, C., Miller, T. E., Jochum, K. P., et al. (2020). Persistent link between Caribbean precipitation and Atlantic Ocean circulation during the Last Glacial revealed by a speleothem record from Puerto Rico. *Paleoceanography and Paleoclimatology*, *35*, e2020PA003944. https://doi.org/10.1029/2020pa003944

Watts, W. A., & Hansen, B. C. S. (1994). Pre-Holocene and Holocene pollen records of vegetation history from the Florida peninsula and their climatic implications. *Paleogeography, Paleoclimatology, Paleoecology*, *109*, 163–176. https://doi.org/10.1016/0031-0182(94)90174-0

Webster, P. J. (2005). The elementary Hadley circulation. In H. F. Diaz, & R. S. Bradley (Eds.), *The Hadley circulation: Present, past and future* (pp. 9–60). Dordrecht: Kluwer.

Weijers, J. W., Schefuß, E., Schouten, S., & Damsté, J. S. S. (2007). Coupled thermal and hydrological evolution of tropical Africa over the last deglaciation. *Science*, *315*(5819), 701–1704. https://doi.org/10.1126/science.1138131

Weldeab, S. (2012). Bipolar modulation of millennial-scale West African monsoon variability during the last glacial (75,000–25,000 yr ago). *Quaternary Science Reviews*, *40*, 21–29. https://doi.org/10.1016/j.quascirev.2012.02.014

Weldeab, S., Lea, D. W., Schneider, R. R., & Andersen, N. (2007). 155,000 yr of West African monsoon and ocean thermal evolution. *Science*, *316*(5829), 1303–1307. https://doi.org/10.1126/science.1140461

Wille, M., Hooghiemstra, H., Behling, H., van der Borg, K., & Negret, A. J. (2001). Environmental change in the Colombian subandean forest belt from 8 pollen records: The last 50 kyr. *Vegetation History and Archaeobotany*, *10*, 61–77. https://doi.org/10.1007/pl00006921

Wu, Y., Li, T. Y., Yu, T. L., Shen, C. C., Chen, C. J., Zhang, J., et al. (2020). Variation of the Asian summer monsoon since the last glacial-interglacial recorded in a stalagmite from southwest China. *Quaternary Science Reviews*, *234*, 106261. https://doi.org/10.1016/j.quascirev.2020.106261

Yancheva, G., Nowaczyk, N. R., Mingram, J., Dulski, P., Schettler, G., Negendank, J. F., et al. (2007). Influence of the intertropical convergence zone on the East Asian monsoon. *Nature*, *445*(7123), 74–77. https://doi.org/10.1038/nature05431

Yang, H., Johnson, K. R., Griffiths, M. L., & Yoshimura, K. (2016). Interannual controls on oxygen isotope variability in Asian monsoon precipitation and implications for paleoclimate reconstructions. *Journal of Geophysical Research: Atmospheres*, *121*(14), 8410–8428. https://doi.org/10.1002/2015jd024683

Yuan, D., Cheng, H., Edwards, R. L., Dykoski, C. A., Kelly, M. J., Zhang, M., et al. (2004). Timing, duration, and transitions of the last interglacial Asian monsoon. *Science*, *304*(5670), 575–578. https://doi.org/10.1126/science.1091220

Zarriess, M., Johnstone, H., Prange, M., Steph, S., Groeneveld, J., Mulitza, S., & Mackensen, A. (2011). Bipolar seesaw in the northeastern tropical Atlantic during Heinrich stadials. *Geophysical Research Letters*, *38*(4), L04706. https://doi.org/10.1029/2010GL046070

Zhang, H., Ait Brahim, Y., Li, H., Zhao, J., Kathayat, G., Tian, Y., et al. (2019). The Asian summer monsoon: Teleconnections and forcing mechanisms—A review from Chinese speleothem $\delta^{18}O$ records. *Quaternary*, *2*(3), 26. https://doi.org/10.3390/quat2030026

Zhang, H., Griffiths, M. L., Chiang, J. C., Kong, W., Wu, S., Atwood, A., et al. (2018). East Asian hydroclimate modulated by the position of the westerlies during Termination I. *Science*, *362*(6414), 580–583. https://doi.org/10.1126/science.aat9393

Zhang, R., & Delworth, T. L. (2005). Simulated tropical response to a substantial weakening of the Atlantic thermohaline circulation. *Journal of Climate*, *18*, 1853–1860. https://doi.org/10.1175/jcli3460.1

Zhang, T.-T., Li, T.-Y., Cheng, H., Edwards, R. L., Shen, C.-C., Spötl, C., et al. (2017). Stalagmite-inferred centennial variability of the Asian summer monsoon in southwest China between 58 and 79 ka B.P. *Quaternary Science Reviews*, *160*, 1–12. https://doi.org/10.1016/j.quascirev.2017.02.003

Zhang, W., Wu, J., Wang, Y., Wang, Y., Cheng, H., Kong, X., & Duan, F. (2014). A detailed East Asian monsoon history surrounding the 'Mystery Interval' derived from three Chinese speleothem records. *Quaternary Research*, *82*(1), 154–163. https://doi.org/10.1016/j.yqres.2014.01.010

Zhao, K., Wang, Y., Edwards, R. L., Cheng, H., & Liu, D. (2010). High-resolution stalagmite $\delta^{18}O$ records of Asian monsoon changes in central and southern China spanning the MIS 3/2 transition. *Earth and Planetary Science Letters*, *298*(1–2), 191–198. https://doi.org/10.1016/j.epsl.2010.07.041

Zhou, Y., McManus, J. F., Jacobel, A. W., Costa, K. M., Wang, S., & Caraveo, B. A. (2021). Enhanced iceberg discharge in the western North Atlantic during all Heinrich events of the last glaciation. *Earth and Planetary Science Letters*, *564*, 116910. (in press). https://doi.org/10.1016/j.epsl.2021.116910

Zorzi, C., Goni, M. F. S., Anupama, K., Prasad, S., Hanquiez, V., Johnson, J., & Giosan, L. (2015). Indian monsoon variations during three contrasting climatic periods: The Holocene, Heinrich Stadial 2, and the last interglacial-glacial transition. *Quaternary Science Reviews*, *125*, 50–60. https://doi.org/10.1016/j.quascirev.2015.06.009